AD_____

Award Number: W81XWH-04-1-0391

TITLE: In Vivo Fluorescence Confocal Microscopy to Investigate the Role of RhoC in Inflammatory Breast Cancer

PRINCIPAL INVESTIGATOR: Michaela Hoffmeyer

CONTRACTING ORGANIZATION: University of Texas at Austin
Austin, TX 78712-1500

REPORT DATE: November 2005

TYPE OF REPORT: Annual Summary

PREPARED FOR: U.S. Army Medical Research and Materiel Command
Fort Detrick, Maryland 21702-5012

REPORT DOCUMENTATION PAGE

Form Approved
OMB No. 0704-0188

1. REPORT DATE *(DD-MM-YYYY)*	2. REPORT TYPE	3. DATES COVERED *(From - To)*
01-11-2005	Annual Summary	5 Mar 04 – 31 Oct 05

4. TITLE AND SUBTITLE
In Vivo Fluorescence Confocal Microscopy to Investigate the Role of RhoC in Inflammatory Breast Cancer

5a. CONTRACT NUMBER

5b. GRANT NUMBER
W81XWH-04-1-0391

5c. PROGRAM ELEMENT NUMBER

6. AUTHOR(S)
Michaela Hoffmeyer

E-Mail: michaelazahn@gmail.com

5d. PROJECT NUMBER

5e. TASK NUMBER

5f. WORK UNIT NUMBER

7. PERFORMING ORGANIZATION NAME(S) AND ADDRESS(ES)
University of Texas at Austin
Austin, TX 78712-1500

8. PERFORMING ORGANIZATION REPORT NUMBER

9. SPONSORING / MONITORING AGENCY NAME(S) AND ADDRESS(ES)
U.S. Army Medical Research and Materiel Command
Fort Detrick, Maryland 21702-5012

10. SPONSOR/MONITOR'S ACRONYM(S)

11. SPONSOR/MONITOR'S REPORT NUMBER(S)

12. DISTRIBUTION / AVAILABILITY STATEMENT
Approved for Public Release; Distribution Unlimited

13. SUPPLEMENTARY NOTES

14. ABSTRACT

Inflammatory breast cancer (IBC) is a highly aggressive form of breast cancer characterized by a dermal inflammatory-like presentation. This phenotype maybe due to a unique method of invasion not well characterized. We have made considerable progress in investigating whether RhoC expression plays a role in the unique phenotype of IBC. Bicistronic red fluorescent protein (RFP) expression vectors containing mutant forms of Rho proteins have been successfully constructed and stable IBC and control breast cancer cell line selection is underway. *In vitro* analysis, submitted for publication, of the SUM 149 (IBC) and the SUM 102 (non-IBC) cell lines has revealed reduced invasion and adhesive capacity to basal lamina components by the IBC cell line, possibly suggesting a passive mode of IBC dissemination. Stably expressing RFP IBC and RFP MDA-MB-435α6HG6 breast cancer cell lines have been constructed and used successfully in the optimization of a macroscopic fluorescence imaging system for utilization in determining tumor take, monitoring tumor growth, and locating sites of invasion for imaging with our confocal *in vivo* fluorescence microscope. Finally, construction of the *in vivo* fluorescence confocal microscope is in process with our collaborators.

15. SUBJECT TERMS
Inflammatory breast cancer, invasion, metastasis, RhoC, Rho GTPases, imaging, mouse models

16. SECURITY CLASSIFICATION OF:			17. LIMITATION OF ABSTRACT	18. NUMBER OF PAGES	19a. NAME OF RESPONSIBLE PERSON
a. REPORT	b. ABSTRACT	c. THIS PAGE			USAMRMC
U	U	U	UU	44	19b. TELEPHONE NUMBER *(include area code)*

Table of Contents

Introduction

IBC is the most lethal and aggressive form of locally advanced breast cancer [1]. The lethality of IBC stems from its highly invasive nature. Complicating treatment of this deadly form of breast cancer is that very little information about the cellular mechanisms responsible for the unique IBC phenotype is known. The recent discovery of the overexpression of the Rho isoform RhoC by IBC tumors has been implicated in the physiological mechanisms of this poorly characterized form of breast cancer [2]. Another unique feature of IBC is the overexpression of E-cadherin, a transmembrane protein involved in cell-cell adhesion, which is generally lost in highly invasive cancers. It seems somewhat paradoxical that such an aggressive cancer that overexpresses proteins involved in actin cytoskeleton rearrangement and promotion of migration (i.e., RhoC) also overexpresses cell-cell junction proteins such as E-cadherin [3-7]. Histological examination of IBC tumors reveals numerous cancer cell emboli within the dermal lymphatics. Such a phenotype might be due to passive dissemination of IBC, rather than active invasion and migration through the basal lamina [8].

Body

We have successfully completed the following two projects in the first year of the award.

Comparative analysis of the invasive phenotype of IBC and non-IBC cell lines:

Using the SUM 149 IBC cell line, we have examined the adhesive and migratory capacities in an effort to understand the invasive behavior of IBC for future experimentation with *in situ* imaging of IBC in animal models. SUM 149 was compared to a control cell line, SUM 102, which was selected because it shares a deletion in the LIBC (lost in inflammatory breast cancer) gene with the SUM 149 cell line but reportedly expresses RhoC mRNA at low levels [2]. We show that SUM 149 is less invasive and adhesive to basal lamina components *in vitro* than SUM 102, and that SUM 149 expresses more Rho proteins and E-cadherin. These data shows that SUM 149 is not highly motile and therefore possibly not actively invasive, suggesting passive metastasis as the mechanism of IBC dissemination. Please see attached manuscript in appendix (Hoffmeyer, et al., Cancer Cell International, 2005, 5:11).

Image analysis of fluorescent breast tumor progression in mouse models:

We have constructed a unique macroscopic *in vivo* imaging system to analyze primary and metastatic tumors that stably express fluorescent markers. This imaging system consists of a Xenon light source reflected through an excitation filter wheel that has filters for red or green fluorescence. Fluorescence emission from cells or tissue can be imaged via a digital camera with attached emission filters for red or green fluorescence (Fig. 1). This system was used to image and quantify the fluorescence intensity of the *in vivo* progression of red fluorescent protein (RFP)-expressing SUM 149 IBC cells as well as a RFP-tagged high metastatic human breast cancer cell line MDA-MB-435α6HG6 (Figs. 2-3). We have successfully followed the breast cancer cells that have the RFP cDNA stably integrated into their genome from the time of injection into the mammary fat pads of female immunocompromised mice up to local invasion and formation of distant lung metastases (Figs. 2-4). This system will aid in determining efficiency of tumor take in our mouse model at an earlier time point than by traditional methods. Furthermore, this macroscopic fluorescence imaging system will be used to future *in vivo* fluorescence confocal imaging studies to non-invasively locate areas of particular interest, such

as sites active invasion, for image analysis. Finally, this system will also be used to investigate the efficacy of phytochemical compounds in the prevention of breast cancer metastasis.

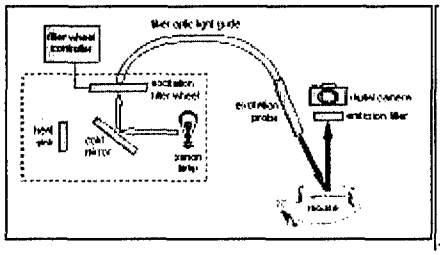

Fig. 1. IBC cells invade as emboli and may exhibit passive metastasis *in vivo*. A 300W Xenon arc lamp with integrated parabolic reflector directs light by a cold mirror to the excitation filter wheel. For RFP, we used a bandpass filter centered at 545nm as our excitation filter. One filter slot is open for white light illumination to image the position of the mouse. Excitation light is focused onto a flexible fiber optic light guide for delivery to the tumor. Fluorescence emission from the tissue is recorded using a Canon EOS-D30 digital camera, with two emission filters attached prior to the camera lens: a bandpass filter centered at 610nm and a 570nm longpass filter. These filters were used to reject scattered or reflected excitation light so only the fluorescence from the sample was imaged by the camera.

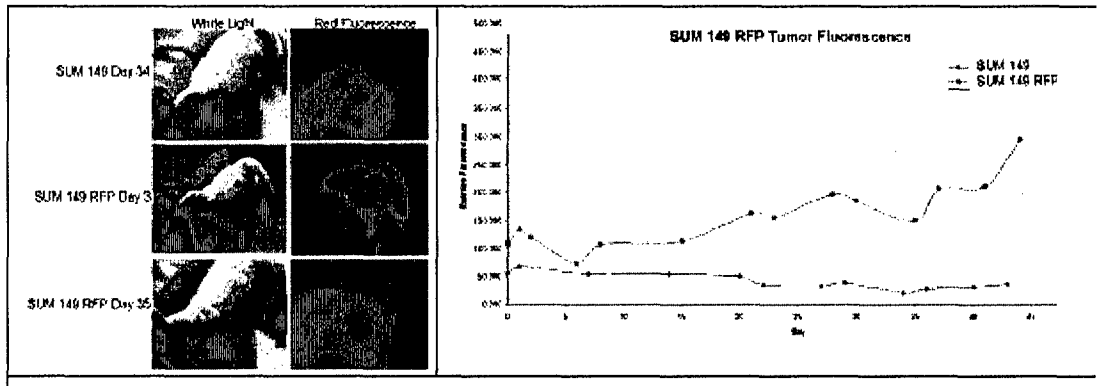

Fig. 2. *In situ* detection of primary breast tumors created with RFP-tagged SUM 149 human breast cancer cells. RFP-tagged SUM 149 cells were injected to the right mammary fat pad of a female SCID mouse and tumor progression was followed using a macroscopic fluorescent imaging system as detailed in Fig.1. Fluorescent breast tumor was imaged non-invasively and quantified by fluorescence intensity (Right Panel).

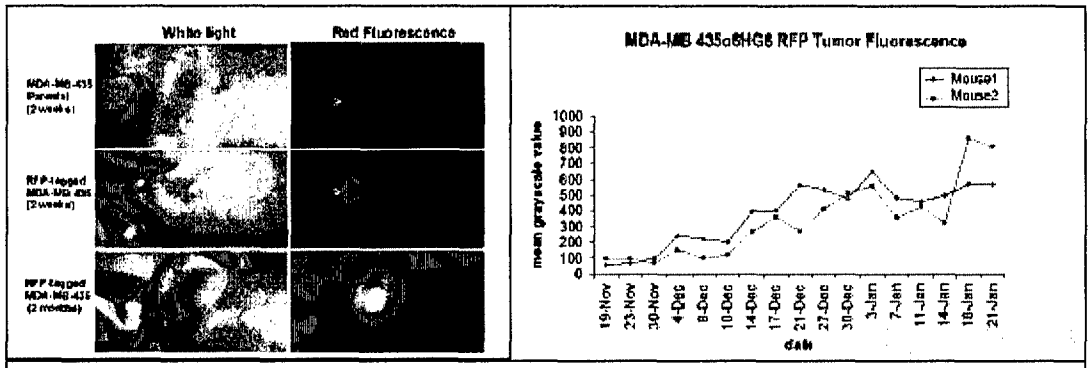

Fig. 3. *In situ* detection of primary breast tumors created with red fluorescent protein (RFP)-tagged MDA-MB-435 human breast cancer cells. RFP-tagged MDA-MB-435 cells were injected to the right mammary fat pad of a female athymic nude mice and tumor progression was followed using a macroscopic fluorescent imaging system as detailed in Fig.1. Fluorescent breast tumor was imaged non-invasively and quantified by fluorescence intensity (Right Panel).

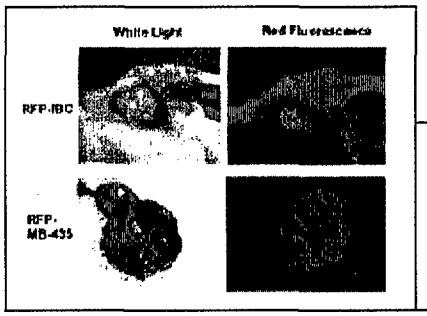

Fig.4. Macroscopic imaging of RFP-expressing breast cancer invasion and metastasis in mice. Top panel, Local invasion of RFP-tagged SUM-149 human inflammatory breast cancer (IBC) cells in SCID mouse, 45 days following inoculation. Bottom Panel, Lung metastases of RFP-tagged MDA-MB-435α6HG6 metastatic human breast cancer cells 75 days following inoculation.

Key Research Accomplishments

• *In vitro* analysis of the invasive phenotypes of SUM 149 (IBC) and SUM 102 (non-IBC) has been accomplished by protein expression analysis of E-cadherin and Rho isoforms, invasion and migration assays, and immunohistochemistry of cytoskeletal structures.

• Construction of bicistronic expression vectors and site-directed mutagenesis: RFP, RhoC, RhoC dominant active, RhoC dominant negative, RhoA dominant active, RhoA dominant negative.

• Construction of stable RFP expressing human breast cancer cell lines SUM 149 RFP and MDA-MB 435α6HG6.

• Construction and optimization of *in vivo* macroscopic fluorescence imaging system: Imaging of RFP tumortake, growth, and metastasis of RFP SUM 149 (IBC) and RFP MDA-MB 435α6HG6 tumors in mice.

Reportable Outcomes

- Our *in vitro* analysis of the unmodified SUM 149 (IBC) and SUM 102 (non-IBC) human breast cancer cell line is complete. This work was recently published in the journal, *Cancer Cell International* 2005, 5:11; Hoffmeyer MR, Wall KM, Dharmawardhane SF. "In vitro analysis of the invasive phenotype of SUM 149, an inflammatory breast cancer cell line."
- Our *in vivo* macroscopic imaging of RFP expressing breast cancer cell lines has been submitted to *Lasers in Medicine and Surgery*. Hoffmeyer MR, Carlson, AL, Wall KM, Baugher PB, Kortum RR, Dharmawardhane SF. "*In situ* analysis of breast cancer progression in murine models using a macroscopic fluorescence imaging system" (see Appendix).

Conclusions

Many of the experiments proposed for the first year in the statement of work have been accomplished.

Task 1. Creation of stable red fluorescent protein (RFP) tagged inflammatory breast cancer (IBC) cell line and control breast cancer cell line expressing dominant negative and dominant active forms of RhoC respectively.

A. Site directed mutagenesis has been preformed on the RhoC cDNA yielding the following mutation:
   I. RhoC(G14V): dominant active
   II. RhoC(T19N): dominant negative
   III. RhoA(G14V): dominant active

B. Mutated Rho cDNA has been subcloned into bicistronic expression vectors

C. Stable RFP expressing breast cancer cell lines containing have been constructed. We have initiated construction of the stable Rho mutant expressing breast cancer cell lines.
   I. SUM 149 (IBC) cells expressing RFP
   II. MDA-MB 435 α6HG6 cells expressing RFP

Task 2. Investigate the invasive mechanism of the RFP breast cancer cell lines expressing mutant RhoC in live mouse tumors.

A. Design and adapt a fluorescence confocal microscope to specifically image RFP RhoC mutant breast cancer cells in mouse tumors is underway by our collaborators in the Biomedical Engineering Department at the University of Texas Austin.

B. RFP expressing cells have been injected into the mammary fat pads of female immunocompromised and tumor take and growth monitored via our macroscopic fluorescence imaging system. Metastases have been visualized via fluorescent signal in mouse models.

Unfortunately, this project could not be completed because both thesis advisors Dr. Su Dharmawardhane and Dr. Rebecca Richards-Kortum left the University of Texas at Austin in August 2005. Therefore, the PI Michaela Hoffmeyer decided to leave the Degree Program with a Masters Degree. The funds for the remaining years of the study are being returned to the Department of Defense.

References

1. Levine PH, Steinhorn SC, Ries LG, Aron JL: Inflammatory breast cancer: the experience of the surveillance, epidemiology, and end results (SEER) program. *J Natl Cancer Inst* 1985, 74: 291-297.

2. van Golen KL, Davies S, Wu ZF, Wang YF, Bucana CD, Root H, Chandrasekharappa S, Strawderman M, Ethier SP, Merajver SD: A novel putative low-affinity insulin-like growth factor-binding protein, LIBC (lost in inflammatory breast cancer), and RhoC GTPase correlate with the inflammatory breast cancer phenotype. *Clin Cancer Res* 1999, 5: 2511-2519.

3. Tomlinson JS, Alpaugh ML, Barsky SH: An intact overexpressed E-cadherin/α,β-Catenin axis characterizes the lymphovascular emboli of inflammatory breast carcinoma. *Cancer Res* 2001, 61: 5231-5241.

4. Alpaugh ML, Tomlinson JS, Kasraeian S, Barsky SH: Cooperative role of Ecadherin and sialyl-Lewis X/A-deficient MUC1 in the passive dissemination of tumor emboli in inflammatory breast carcinoma. *Oncogene* 2002, 21: 3631-3643.
5. Alpaugh ML, Tomlinson JS, Shao ZM, Barsky SH: A novel human xenograft model of inflammatory breast cancer. *Cancer Res* 1999, 59: 5079-5084.
6. Colpaert CG, Vermeulen PB, Benoy I, Soubry A, van Roy F, van Beest P, Goovaerts G, Dirix LY, van Dam P, Fox SB, Harris AL, van MarckEA: Inflammatory breast cancer shows angiogenesis with endothelial proliferation rate and strong E-Cadherin expression. *Br J Cancer* 2003, 10: 718-725.
7. Kleer CG, van Golen KL, Braun T, Merajver SD: Persistent E-cadherin expression in inflammatory breast cancer. *Mod Pathol* 2001, 14: 458-464.
8. Cavallaro U, Christofori G: Cell adhesion in tumor invasion and metastasis: loss of the glue is not enough. *Biochimica et Biophysica Acta* 2001, 1552: 39-45.

Appendix

Hoffmeyer MR, Wall KM, Dharmawardhane SF. 2005. "In vitro analysis of the invasive phenotype of SUM 149, an inflammatory breast cancer cell line." *Cancer Cell International* 5:11.

Hoffmeyer, M.R, Carlson, A.L, Wall, K., Richards-Kortum, R., **Dharmawardhane, S.** "*In situ* analysis of breast cancer progression in murine models using a macroscopic fluorescence imaging system". Submitted, *Lasers in Medicine and Surgery*.

Cancer Cell International

CANCER CELL INTERNATIONAL

BioMed Central

Primary research

Open Access

In vitro analysis of the invasive phenotype of SUM 149, an inflammatory breast cancer cell line

Michaela R Hoffmeyer[1], Kristin M Wall[2] and Suranganie F Dharmawardhane*[1]

Address: [1]Department of Molecular Cell and Developmental Biology, University of Texas Austin, 205 West 24th Street, Austin, Texas, 78712, USA and [2]Department of Biomedical Engineering, University of Texas at Austin, 1 University Station Stop C0800, Austin, TX 78712, USA

Email: Michaela R Hoffmeyer - mrhoffmeyer@hotmail.com; Kristin M Wall - kmariew@hotmail.com; Suranganie F Dharmawardhane* - surangi@mail.utexas.edu

* Corresponding author

Published: 27 April 2005

Cancer Cell International 2005, **5**:11 doi:10.1186/1475-2867-5-11

Received: 15 November 2004
Accepted: 27 April 2005

This article is available from: http://www.cancerci.com/content/5/1/11

Abstract

Background: Inflammatory breast cancer (IBC) is the most lethal form of locally invasive breast cancer known. However, very little information is available on the cellular mechanisms responsible for manifestation of the IBC phenotype. To understand the unique phenotype of IBC, we compared the motile and adhesive interactions of an IBC cell line, SUM 149, to the non-IBC cell line SUM 102.

Results: Our results demonstrate that both IBC and non-IBC cell lines exhibit similar adhesive properties to basal lamina, but SUM 149 showed a marked increase in adhesion to collagen I. *In vitro* haptotaxis assays demonstrate that SUM 149 was less invasive, while wound healing assays show a less *in vitro* migratory phenotype for SUM 149 cells relative to SUM 102 cells. We also demonstrate a role for Rho and E-cadherin in the unique invasive phenotype of IBC. Immunoblotting reveals higher E-cadherin and RhoA expression in the IBC cell line but similar RhoC expression. Rhodamine phalloidin staining demonstrates increased formation of actin stress fibers and larger focal adhesions in SUM 149 relative to the SUM 102 cell line.

Conclusion: The observed unique actin and cellular architecture as well as the invasive and adhesive responses to the extracellular matrix of SUM 149 IBC cells suggest that the preference of IBC cells for connective tissue, possibly a mediator important for the vasculogenic mimicry via tubulogenesis seen in IBC pathological specimens. Overexpression of E-cadherin and RhoA may contribute to passive dissemination of IBC by promoting cell-cell adhesion and actin cytoskeletal structures that maintain tissue integrity. Therefore, we believe that these findings indicate a passive metastatic mechanism by which IBC cells invade the circulatory system as tumor emboli rather than by active migratory mechanisms.

Background

With an average five-year post-recovery survival rate of 45%, inflammatory breast cancer (IBC) is the most lethal and aggressive form of locally advanced breast cancer [1]. The lethality of IBC stems from its highly invasive nature. Diagnosis of IBC is often complicated by lack of a palpable precursor lesion commonly associated with breast cancer. Moreover, the correct diagnosis is hindered by

inflammatory-like symptoms such as redness, warmth, and edema. Characteristic of IBC is a change in breast skin texture, similar to that of an orange, due to extensive invasion of the dermal lymphatics by IBC tumor cell emboli. These complications contribute to IBC lethality in that by the time a proper diagnosis is made, the cancer has aggressively infiltrated the surrounding tissue and lymphatics system, leading to a lowered patient prognosis [2]. Complicating treatment of this deadly form of breast cancer is that very little information about the cellular mechanisms responsible for the unique IBC phenotype is known.

Cancer cell invasion through the basal lamina and subsequent metastasis involves multiple steps including intravasation through the surrounding tissue into the lymphatic or vascular systems. Transient adhesion to extracellular matrix (ECM) components as well as modification of cell shape by reorganization of the actin cytoskeleton is required for cancer cell infiltration into the adjacent tissue. The Rho GTPases regulate actin cytoskeletal rearrangements, and are thus likely candidates for involvement in cancer cell invasion and metastasis [3,4]. Further evidence for a relationship between cancer cell mobilization and dysregulation of Rho GTPases is seen in the overexpression of Rho proteins in numerous invasive human cancers. The recent discovery of the overexpression of the Rho isoform RhoC by IBC tumors has been implicated in the physiological mechanisms of this poorly characterized form of breast cancer [5]. RhoC was demonstrated to be overexpressed in metastatic tumors of pancreatic adenocarcinoma patients [6], murine melanomas [7], and in the patient-derived IBC cell line SUM 149 [5]. Transient inhibition of RhoC in IBC cells by treatment with farnesyl transferase inhibitors reduced invasion and motility *in vitro* [8]. Recently it was reported that RhoC overexpression in mammary epithelial cells resulted in a significant increase in cell migration [9], mediated by the MAPK pathway [10]. These findings led us to hypothesize that RhoC overexpression may promote the highly invasive phenotype of IBC and contribute to the uniquely aggressive phenotype exhibited by IBC.

Another unique feature of IBC is the overexpression of E-cadherin, a transmembrane protein involved in cell-cell adhesion, which is generally lost in highly invasive cancers. It seems somewhat paradoxical that such an aggressive cancer that overexpresses proteins involved in actin cytoskeleton rearrangement and promotion of migration (i.e., RhoC) also overexpresses cell-cell junction proteins such as E-cadherin [11-15]. The literature thus far seems to hold to two schools of thought about the contradictory protein expression seen in IBC. One tends to support the idea that E-cadherin expression fluctuates with disease progression and decreases as IBC cells become invasive [15]. The second school supports the theory of passive metastasis by IBC [11,12]. In passive metastasis, strong tumor cell-cell adhesions are maintained during dissemination that proceeds via vasculogenesis through secretion of differentiation factors by the tumor cells causing *de novo* vessel formation [16]. This results in a cancer cell cluster within the vessel, reminiscent of the IBC tumor emboli seen in IBC histology. Furthermore, RhoC overexpression in human mammary epithelial cells has been shown to increase production of angiogenic factors, some of which might mediate passive or active metastasis [17].

The IBC phenotype has mystified clinicians due to its inflammatory-like symptoms. However IBC symptomology is not considered to be a true immunoreaction, but rather a consequence of cancer cell invasion to the lymphatics system. The mechanism by which IBC invades is unclear and further experimentation with IBC models is required to clarify the exact mechanism by which this form of breast cancer is disseminated. Using the SUM 149 IBC cell line, we have examined the adhesive and migratory capacities in an effort to understand the invasive behavior of IBC for future experimentation with *in situ* imaging of IBC in animal models. SUM 149 was compared to a control cell line, SUM 102, which was selected because it shares a deletion in the LIBC (lost in inflammatory breast cancer) gene with the SUM 149 cell line but reportedly expresses RhoC mRNA at low levels [5]. We show that SUM 149 is less invasive and adhesive to basal lamina components *in vitro* than SUM 102, and that SUM 149 expresses more Rho proteins and E-cadherin. These data shows that SUM 149 is not highly motile and therefore possibly not actively invasive, suggesting passive metastasis as the mechanism of IBC dissemination.

Results

Endogenous Levels of Rho

Figure 1A presents the relative protein levels of the various Rho isoforms in the IBC cell line SUM 149 versus the non-IBC cell line SUM 102. Previous investigators have reported overexpression of RhoC mRNA in IBC cells compared to SUM 102 [5]. To verify overexpression of RhoC at the protein level, we preformed Western blots on cell lysates using a RhoC polyclonal antibody (Santa Cruz Biotechnology, CA). We found no significant difference in RhoC protein levels between the SUM 149 and the SUM 102 cell lines. However, immunoblotting revealed a significant difference in Rho (A, B, and C), with the IBC cell line expressing much higher Rho protein levels. We then examined RhoA protein levels and found a significant overexpression of RhoA in the IBC cell line. This finding is interesting considering that RhoA has been shown to play a vital role in actomyosin-mediated contractility [21,24].

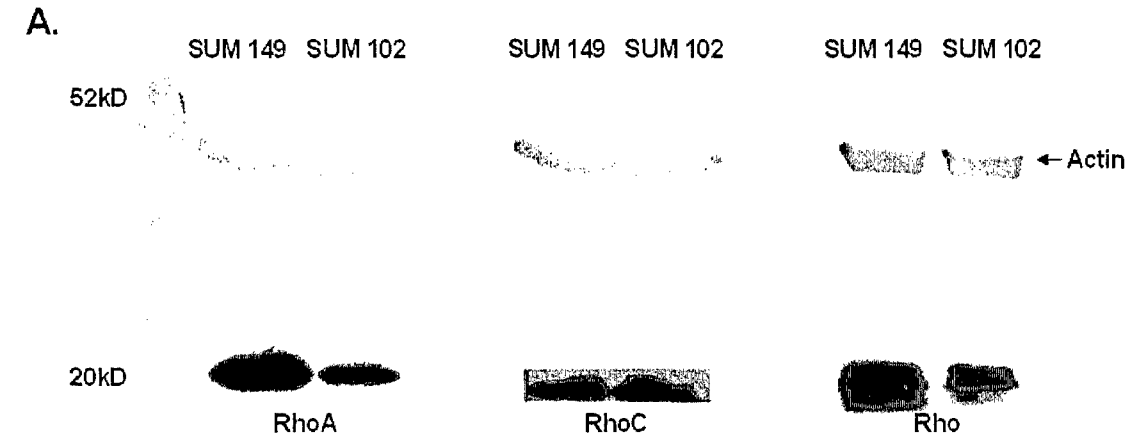

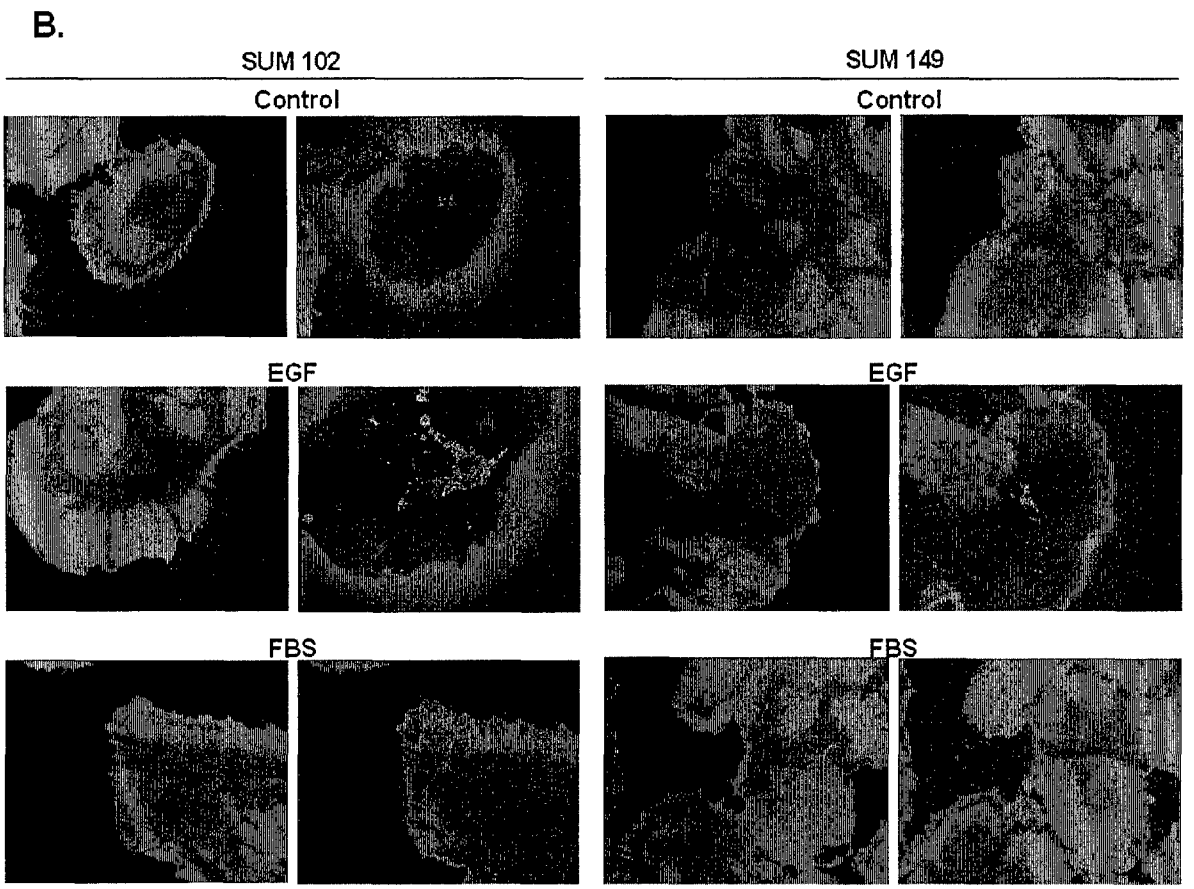

Figure 1

1A. Rho GTPase protein expression levels in the IBC cell line SUM 149 versus SUM 102. 1B. F-actin and focal adhesion distribution in SUM 149 and SUM 102 human breast cancer cell lines. 1A. Equal protein amounts were separated by 10% SDS-PAGE, transferred to nitrocellulose, and probed for RhoA, RhoC, and Rho (A, B, and C). Images are representative of at least three independent experiments with actin serving to verify equal protein loading. 1B. SUM 149 and SUM 102 cells were starved in unsupplemented F-12 Hams media for 24 hours and stimulated for 10 minutes with PBS (control), EGF (50 ng/ml), or FBS (5%). Cells were stained with rhodamine phalloidin (red) to visualize F-actin and anti-phosphotyrosine (green) to visualize focal adhesion. Micrographs were taken at 1000× magnification. Images are representative for at least three independent experiments.

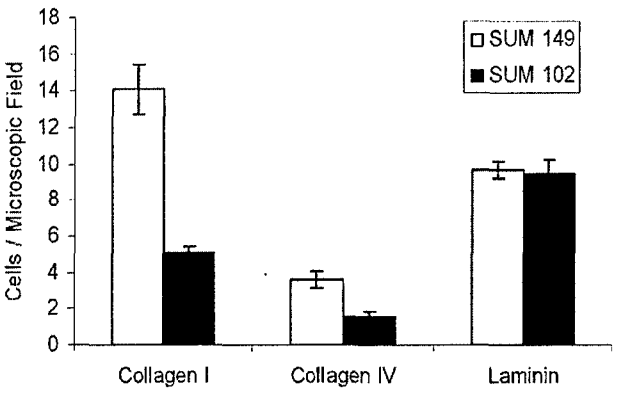

Figure 2
Adhesion of human breast cancer cells to extracellular matrix proteins. SUM 149 and SUM 102 cells (10^5) were plated on glass coverslips coated with laminin (50 μg/ml), collagen I (10 μg/ml), or collagen IV (10 μg/ml) and allowed to adhere for 15 minutes. Micrographs were taken at 400× magnification. Adherent cells were quantified in 10 random microscopic fields. Data are expressed as mean ± SEM of at least three independent experiments.

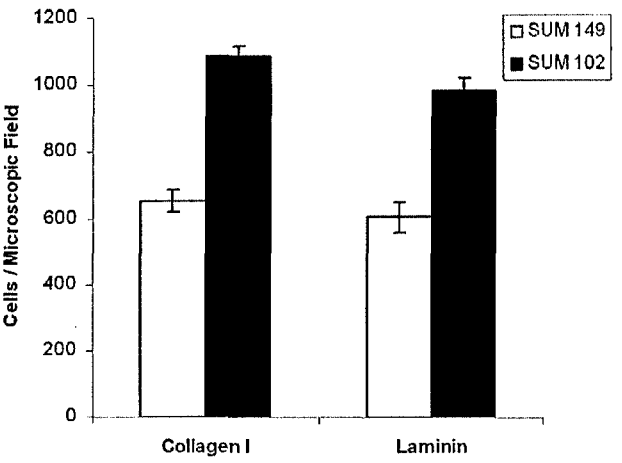

Figure 3
Haptotaxis of human breast cancer cells to extracellular matrix proteins. SUM 149 and SUM 102 cells (10^5) were placed into the top chamber of a Costar well coated with laminin (50 μg/ml) or collagen I (10 μg/ml) and allowed to invade for 24 hours. Invasive cells were stained with propidium iodide and quantified in 10 random microscopic fields. Micrographs were taken at 200× magnification. Data are expressed as mean ± SEM of at least three independent experiments.

Subcellular Distribution of Focal Adhesions and Filamentous Actin

Because RhoA is involved in actin stress fiber and focal adhesion formation, we stained the cells with rhodamine phalloidin to visualize F-actin and anti-phosphotyrosine to visualize focal adhesions. Figure 1B demonstrates F-actin and focal adhesion distribution in both cell lines. SUM 149 displayed larger focal adhesions and more actin stress fibers than the SUM 102 cell line, as might be expected from the high levels of RhoA in the SUM 149 cell line. Upon stimulation of quiescent cells with EGF or FBS, the SUM 102 cells formed large membrane ruffles (lamellipodia). However, stimulation by both EGF and FBS seemed to have little effect on the actin cytoskeleton of the SUM 149 cells. An increase in focal adhesion was seen in the SUM 149 cells after stimulation with EGF, but no clear cell polarization was observed.

Adhesion to Extracellular Matrix Proteins

Invasion and metastasis is a multi-step process in which cells must break local connections, move through the basal lamina, survive in circulation, and reestablish cellular attachment at distant sites. Clearly, many of these steps involve interaction with ECM components. Transient adhesion to the ECM in conjunction with cytoskeletal rearrangements are requirements for cell motility. To examine the ability of the breast cancer cell lines under study to adhere to the various ECM proteins, we performed adhesion assays (Figure 2). Here, we demonstrate that both SUM 149 and SUM 102 cells have similar adhesive properties on laminin, the major component of the basal lamina. A slight increase in adhesive properties for the IBC cells was observed compared to the SUM 102 cells on collagen IV. However, a marked increase in adhesion to collagen I, the major component of connective tissue, was seen for the SUM 149 cell line. Taken together, this data suggest that the exacerbated invasive phenotype seen in IBC is not due to differences in adhesive properties to basal lamina components, but may indicate a preference of IBC cells to the connective tissue, through which these cells must invade before entering circulation. Furthermore, attachment to connective tissue components maybe important for vasculogenic mimicry via tubulogenesis, as seen in IBC pathological specimens [25-27].

Haptotaxis Stimulated Invasion

An aggressively infiltrative cancer must invade surrounding tissue by movement through the ECM. Haptotaxis, or cell movement toward ECM proteins, was assayed *in vitro* and is presented in Figure 3. SUM 149 cells were significantly less invasive into laminin (basal lamina component) and collagen I (connective tissue component) after 24 hours than the SUM 102 cell line. Therefore, SUM 149

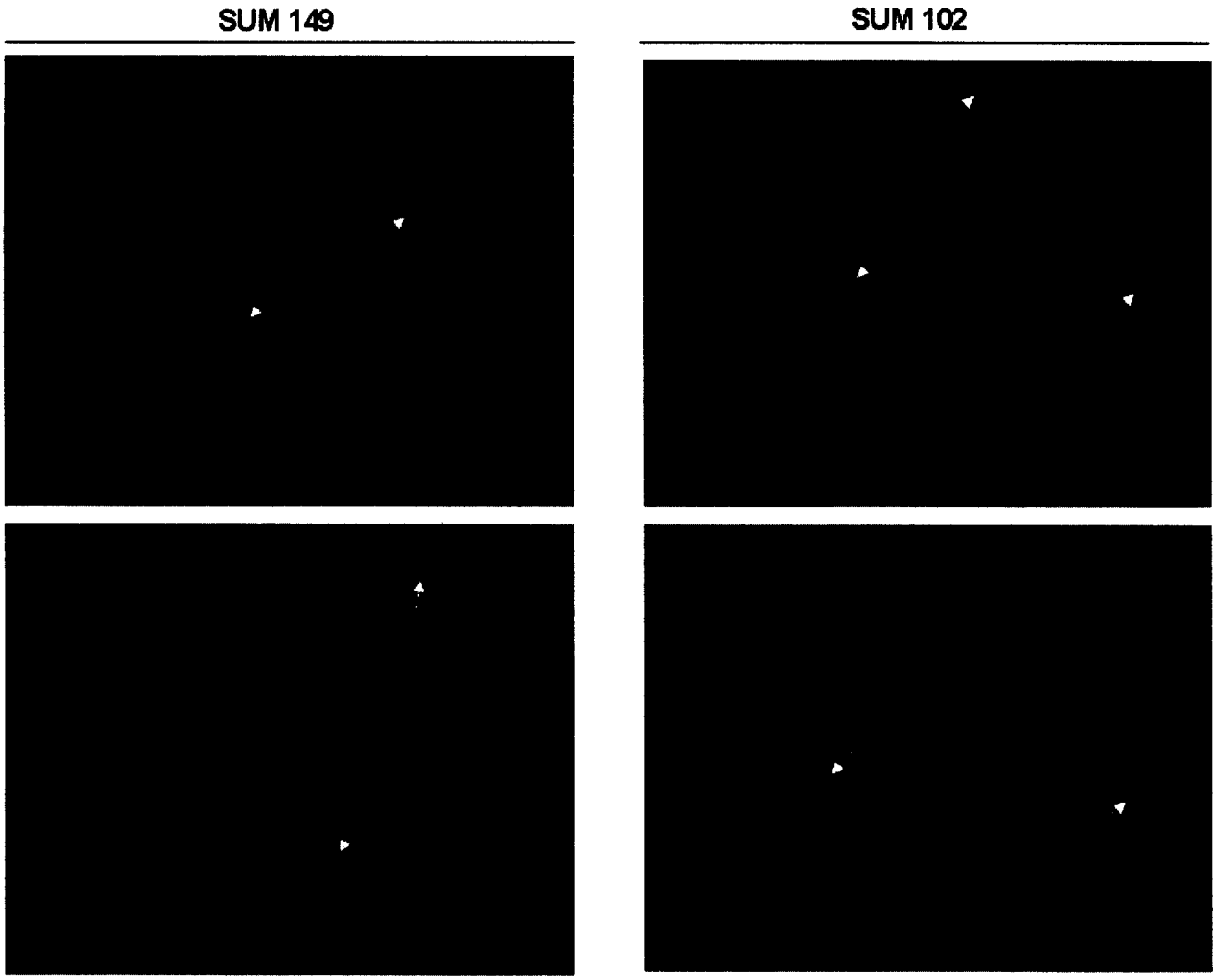

Figure 4
Human breast cancer cell migration in response to wounding. SUM 149 and SUM 102 cells were grown to confluency on glass coverslips and wounded with a sterile razor blade. Closure of the wound was monitored over 7.5 hours. Cells were stained with rhodamine phalloidin to visualize F-actin reorganization in response to cell migration. Arrows indicate the wound edge. Micrographs were taken at 1000× magnification. Images are representative of at least three independent experiments.

was less invasive when assayed in a manner that requires individual cell movement by an active motile mechanism through a membrane with 8 μm pores.

Subcellular Distribution of Filamentous Actin Subsequent to Cellular Polarization

To induce cell polarization and migration that does not involve active migration of individual cells but rather collective cell migration over a wound edge, we performed wound healing assays as described in [28]. A confluent monolayer of cells was wounded, leading to the release of chemotractant signals by the cells at the wound edge, thus mimicking cell motility cues *in vivo* (Figure 4). Here, we present that the IBC cell line SUM 149 was less responsive to the cell-derived migration signals after 7.5 hours. By this time, the SUM 102 cell line was much more invasive into the wound space and had nearly closed the wound entirely. Thus, active migration as a sheet of cells is not likely the mechanism by which IBC is disseminated.

Endogenous Expression of E-cadherin

An interesting and perplexing characteristic of IBC is the expression of E-cadherin by this invasive form of breast cancer. Usually the loss of E-cadherin correlates with

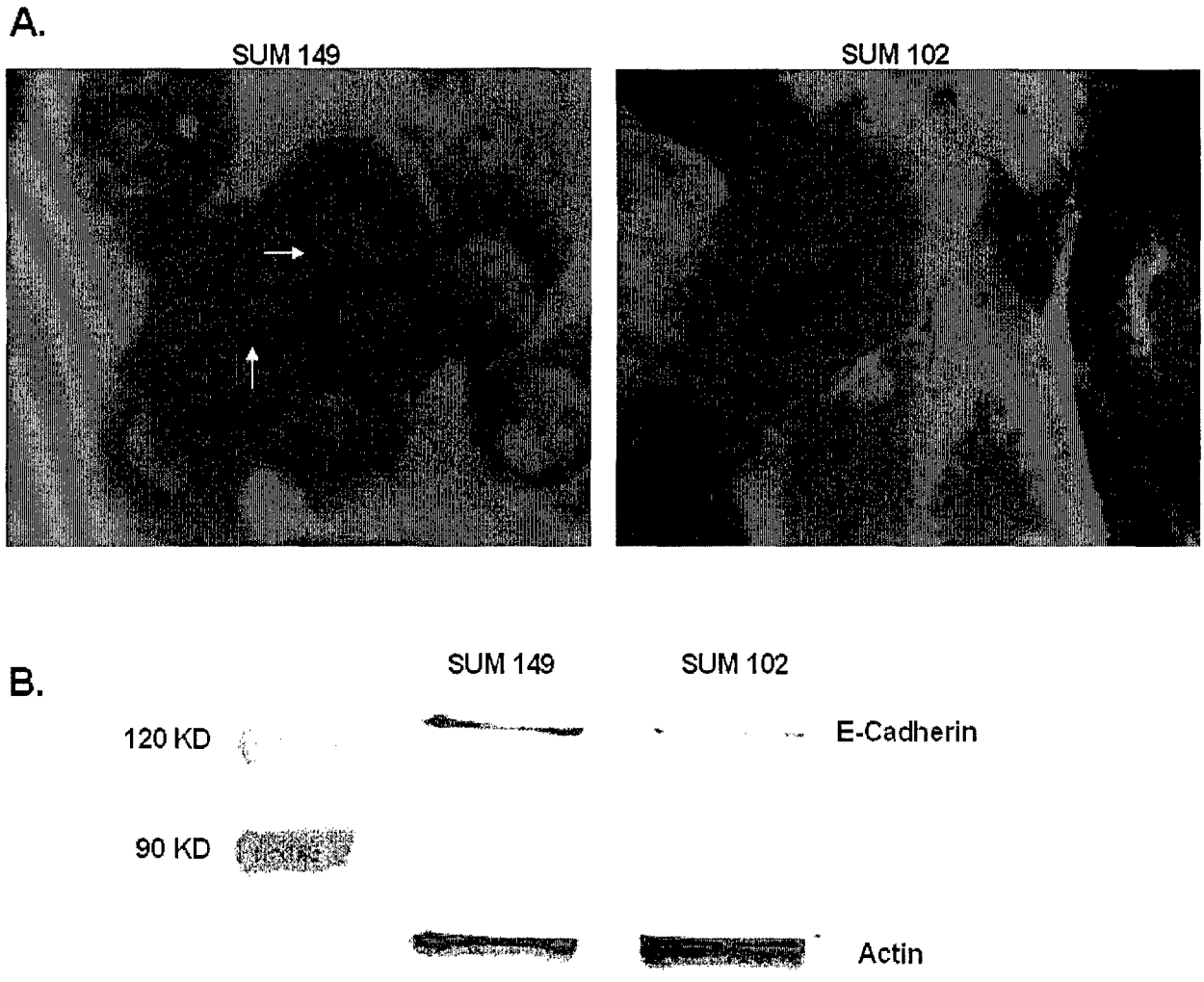

Figure 5
5A. E-cadherin distribution in SUM 149 and SUM 102 human breast cancer cells. 5B. E-cadherin protein expression levels in the IBC cell lineSUM 149 versus SUM 102. 5A. Cells were grown to 60% confluency and stained with anti-E-cadherin (green). Arrows indicate cell-cell adhesions containing E-cadherin. Micrographs were taken at 1000× magnification. Images are representative for at least three independent experiments. 5B. Cell lysates were separated by 8% SDS-PAGE, transferred to nitrocellulose, and probed for E-cadherin. Images are representative of at least three independent experiments with actin serving to verify equal protein loading.

increased invasive and metastatic potential [29]. To verify E-cadherin expression in the IBC cell line SUM 149, we performed immunofluorescence experiments (Figure 5A). Both SUM 149 and SUM 102 show E-cadherin staining localized to the shared margins between neighboring cells, however this staining is much more intense in the SUM 149 cell line. Immunoblotting analysis likewise demonstrates E-cadherin expression by both cell lines with higher levels of E-cadherin expressed in the SUM 149 cells (Figure 5B).

Discussion

IBC is a unique and highly aggressive form of locally advanced breast cancer with distinct clinical presentation. We hypothesized that upregulated expression of RhoC, as reported by others to be characteristic of IBC, contributes to the unusual pathological presentation of IBC. For the first time, we have compared the actin architecture, invasive, and adhesive properties of the IBC cell line SUM 149 with a cell line reported to express less RhoC mRNA compared to SUM 149 but share a deletion in LIBC [5]. Using

a commercially available specific antibody to RhoC, we report that RhoC is not overexpressed at the protein level by the IBC cell line SUM 149. Interestingly, we confirmed overexpression of RhoA by utilizing an anti-RhoA specific antibody. However, post-transcriptional regulation of RhoC expression may account for the observed discrepancy. It is possible that our results do not agree with the reported mRNA expression due to specificity problems with the commercially developed antibodies. Furthermore, we demonstrate that, compared to SUM 102, SUM 149 is less invasive and migratory, and displays impaired adhesion to basal lamina components but strong adhesion to connective tissue proteins.

The role of the Rho protein in cancer cell invasion is somewhat controversial. RhoA is known to be involved in cell contractility, both in the formation of bundled actin fibers and through the activation of Rho kinase and subsequent activation of myosin light chain [30]. Such contractile cells have previously been shown to be less motile [31]. However, Rho overexpression has been documented in various human cancers such as bladder and ovarian, and correlates with lymph node invasion, metastasis, and poor patient prognosis [32,33]. Overexpression of RhoC by human mammary epithelial cells increased invasion, motility, and anchorage independent growth, similar to SUM 149 [9]. Expression of dominant negative Rho T19N has been demonstrated to block melanoma cell invasion [34]. Some investigators report that Rho overexpression has little impact on invasion and cell motility, while others demonstrate a positive correlation between Rho expression and cell migration capacity [35-37]. Rho is required for cell body contraction and tail retraction during directed cell motility, while active Rac and Cdc42 are required for lamellipodia and filopodia extension at the leading edge [30]. Thus, invasive potential is considered to be a balance between Rac, Cdc42, and Rho activities. Overexpression or activation of one of these Rho GTPases will shift this balance and result in a cellular phenotype dominated by the actin structure promoted by the activated Rho GTPase [38]. SUM 149 may display reduced invasion and migration *in vitro* compared to SUM 102 due to the overexpression of RhoA alone, thus masking the motile effects of Rac and Cdc42.

Another aspect that makes IBC so remarkable is that this form of aggressive breast cancer maintains strong E-cadherin expression [11-15]. Typically, loss of E-cadherin expression correlates with progression to metastatic disease since cancer cells must break inter-cell adhesions before attaining a motile phenotype [29]. Here, we demonstrate that the SUM 149 model of IBC maintains strong E-cadherin expression in culture, as seen in other IBC xenograft models and IBC pathological specimens. Previous reports indicate the E-cadherin axis is also complete and functional [11]. IBC histology reveals an extensive invasion of E-cadherin positive tumor cell emboli within the dermal lymphatics [11-15]. The expression of E-cadherin may be critical for invasion in that IBC is thought by some to be passively disseminated, an invasion mechanism that necessitates cell-cell attachment [12]. In this scenario, tumor cells maintain strong cell-cell connections and enter circulation via vasculogenesis around a tumor cell embolus. Others hold that E-cadherin expression varies with the malignant stage of the disease, and is lost during invasion but reestablished once tumor cells invade the vasculature [15]. The finding reported here, in which the IBC cell line SUM 149 was less invasive and adhesive *in vitro* compared to the reportedly less aggressive breast cancer cell line SUM 102, seems to support an alternative mode for IBC dissemination from classic actin cytoskeleton- mediated cell motility.

The high expression levels of both E-cadherin and RhoA by SUM 149 may contribute to the uniquely invasive phenotype of IBC. However, signaling via E-cadherin to Rho is unclear with E-cadherin-mediated Rho activation and inhibition reported in a cell line specific manner [39]. Dominant negative RhoA expression in EL and nEαCL cells has been reported to reduce E-cadherin activity [40]. During the embryonic development of stratified epithelium, it was found that α-catenin, Rho, and Rho kinase were vital for coordinated tissue movement. In this sense, cells maintain tissue architecture via cadherin binding but move as a unit through actin reorganization mediated by Rho and its downstream effector Rho kinase [41]. A parallel argument could be made for the dissemination of IBC, in which tightly bound tumor cells move as a coordinated front. This possibility was tested in a wound healing assay, in which we found that the SUM 149 cells do not polarize or move into the wound after 7.5 hours, suggesting that this form of invasion is not the mechanism by which IBC is dissemination.

Conclusion

Thus, our results demonstrate that the IBC cell line SUM 149 is less invasive than a similar cell line, SUM 102, which expresses less Rho. This finding seems to support an alternate mode of dissemination for IBC than that of the classic invasive model, in which individual cells break local attachments and move through the ECM via actin cytoskeleton remodeling. A previously hypothesized mode of invasion for IBC, termed passive metastasis, would then seem the likely candidate (Figure 6A). In passive metastasis, vasculogenesis, stimulated by secreted differentiation factors, occurs around a tumor cell embolus that has maintained strong cell-cell attachments [16]. IBC is known to secrete angiogenic and possibly also vasculogenic growth factors, such as VEGF, bFGF, IL-6, and IL-8 [17]. Vasculogenic tubule formation by

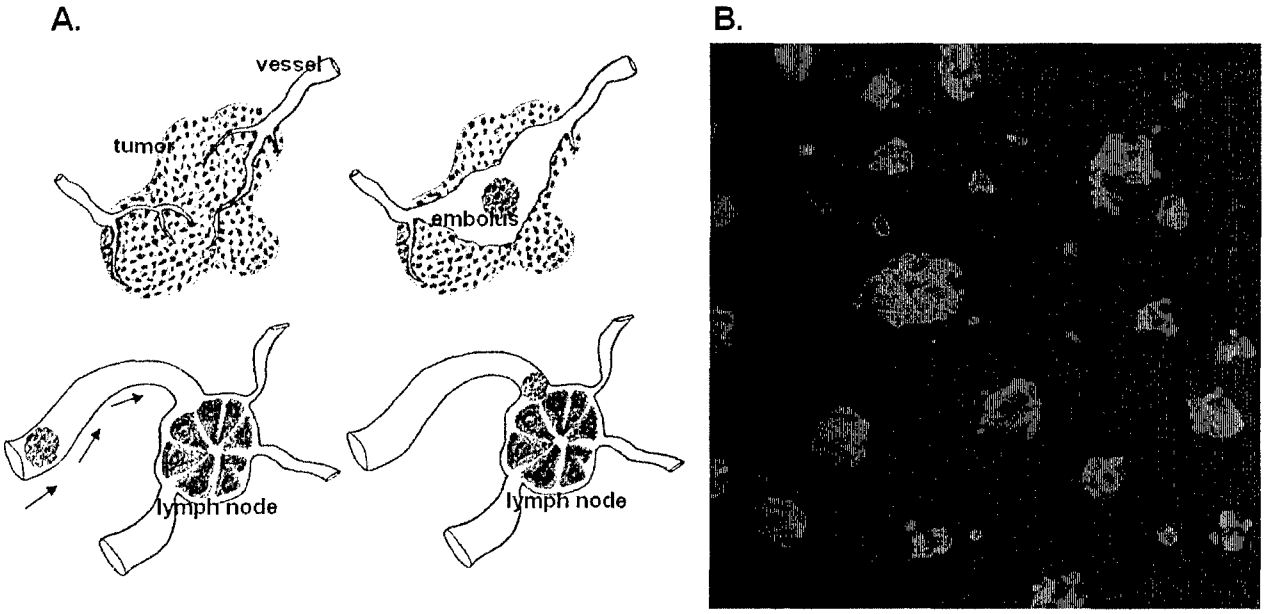

Figure 6

6A. Model of passive metastasis. 6B. SUM 149 cell spheroids expressing RFP. 6A. Tumor cells secrete unknown differentiation factors, stimulating vasculogenesis and resulting in a cluster of tumor cells, termed embolus, located within the *de novo* formed vessel. The embolus maintains cell-cell attachments as it moves through the vessel and lodges within a dermal lymph node. 6B. 100× confocal projection image (10 images, Z = 20 μm) of SUM 149 cell spheroids stably expressing RFP in 3-dimensional matrigel culture after 5 days.

melanoma cells has been shown to be dependent on cadherin expression [42]. E-cadherin positive tumor cell emboli located within the dermal lymphatics are typically found in IBC histological specimens [15]. Three-dimensional culture of SUM 149 cells in matrigel results in IBC cell spheroids that are reminiscent of the tumor cell emboli seen in pathology (Figure 6B). The probability that IBC cells invade the circulatory system by a passive metastasis mechanism as tumor emboli rather than by active migratory mechanisms is being tested by *in vivo* image analysis of fluorescent protein tagged SUM 149 mammary tumors in SCID mice. This investigation could drastically change the course of IBC treatment and identify new therapeutic targets specific for this form of breast cancer.

Methods

Cell Culture

The SUM cell lines used for the study have been recently developed from pleural effusions of breast cancer patients [18,19] and are generous gifts of Dr. Stephen Ethier, The University of Michigan, MI. SUM 149 is an IBC cell line that lacks expression of the gene LIBC and overexpresses RhoC [5]. SUM 102, developed from a minimally invasive human breast carcinoma [20] will be used as a model for non-IBC human breast cancer cells. SUM 149 cells were cultured in F-12 Hams (Gibco™, CA) supplemented with 5% fetal bovine serum (Tissue Culture Biologicals, CA), insulin, and hydrocortisone. SUM 102 cells were cultured in F-12 Hams (Gibco™, CA) supplemented with 5% bovine serum albumin (BSA), epidermal growth factor, T3, ethanolamine, and sodium selenite.

Adhesion Assays

Cell adhesion assays were performed according to [21]. Briefly, glass coverslips (Fisher Scientific, TX) were coated with 50 μg/ml laminin (Gibco BRL, MD), 10 μg/ml of collagen I (BD Biosciences, MA), 10 μg/ml of collagen IV (BD Biosciences, MA) and incubated overnight at 4°C. The coverslips were blocked for 1 hour with 1% heat-denatured BSA (Sigma Chemical Corporation, MO) in PBS. Cells (10^5) were placed on coverslips and allowed to adhere for 15 minutes. Non-adherent cells were removed by washing. The adherent cells were fixed in 3.7% formaldehyde (Sigma Chemical Corp., MO) and stained for F-actin as described below to aid in quantification. The number of cells per coverslip was quantified with a 40× phase contrast objective.

Haptotaxis Invasion Assay

Cell invasion assays were performed as described in [22]. Modified Boyden chambers (tissue culture treated, 6.5 mm diameter, 10 μm thickness, 8 μm pores, Transwell®, Costar Corp., Cambridge, MA) were coated on the upper surface (invasion), of the membrane with 50 μg/ml laminin, 10 μg/ml collagen I, or 10 μg/ml collagen IV overnight at 4°C and then placed into the lower chamber containing 500 μl culture media with 10% fetal bovine serum (FBS). Serum starved cells (10^5) were added to the upper surface of each migration chamber and allowed to migrate to the underside of the membrane for 24 hours (invasion). The non-migratory cells on the upper membrane surface were removed with a cotton swab, and the migratory cells attached to the bottom surface of the membrane stained with propidium iodide (CalBioChem-Novabiochem Corp., CA). The number of invasive cells per membrane was counted with an Olympus upright fluorescence microscope with a 40× objective.

Wound Healing Assay

Cells were first grown to a confluent monolayer, wounded with a sterile razor blade and allowed to migrate for 7.5 hours before fixing, permeabilizing, and blocking. Cells were then stained for F-actin as described below and visualized using an Olympus upright fluorescence microscope.

Immunofluorescence Microscopy

For focal adhesion and F-actin staining, cells were cultured on coverslips until they reached 60% confluency and starved for 24 hours in unsupplemented F-12 Hams. Cells were then stimulated with 50 ng/ml epidermal growth factor (EGF), 5% FBS, or PBS control for 10 minutes, fixed in 3.7% formaldehyde (Sigma Chemical Corp., MO), permeabilized with 0.2% Triton X-100 (Sigma, MO), and blocked with 5% goat serum (Gibco™, CA), and 5% BSA (Sigma Chemical Corp., MO) in PBS. Cells were stained with rhodamine phalloidin (Molecular Probes Inc., OR) to visualize F-actin, and a mouse monoclonal anti-phosphotyrosine antibody, clone 4G10 (Upstate Biotechnology, NY), followed by FITC-conjugated goat anti mouse IgG (ICN Biomedicals Inc., CA) to visualize the focal adhesions. Phosphotyrosine staining to is commonly utilized to visualize focal adhesions [23]. For E-cadherin staining, cells were cultured until 60% confluency, fixed in methanol at -20°C for 15 minutes, and blocked with 5% goat serum (Gibco™, CA) and 5% BSA (Sigma Chemical Corp., MO) in PBS. Cells were stained with a mouse monoclonal anti-E-cadherin antibody, clone G-10 (Santa Cruz Biotechnology, CA) followed by FITC-conjugated goat anti-mouse IgG (ICN Biomedicals Inc., CA). Cells were imaged using an Olympus upright fluorescence microscope with Spot Advanced digital camera software, Version 2.2.1 (Diagnostic Instruments Inc., MI).

Immunoblotting

Cells were cultured to confluency on 6 cm plates, trypsinized and the pellet washed in 1X PBS. The cell pellet was then lysed in 1% NP-40 lysis buffer. Equal amounts of protein, as determined by Bio-Rad (Hercules, CA) total protein assay, were then separated by 10% SDS-PAGE gel for Rho (A, B, and C), RhoA, and RhoC, or 8% SDS-PAGE gel for E-cadherin. Cellular proteins were then transferred to a nitrocellulose membrane. Membranes were blocked with 4% milk 0.05% Tween and probed with rabbit polyclonal anti-Rho (A, B, and C) (Upstate Biotechnology, NY), mouse monoclonal anti-RhoA (Santa Cruz Biotechnology, CA), goat polyclonal anti-RhoC (Santa Cruz Biotechnology, CA), or mouse monoclonal anti-E-cadherin (Santa Cruz Biotechnology, CA) followed by horseradish peroxidase-conjugated goat anti-mouse antibody (Pierce Endogen, IL) for Rho or alkaline phosphatase conjugated goat anti mouse antibody for E-cadherin (Pierce Endogen, IL). Rho immunoblots were detected with the Super Signal West Femto-Substrate chemiluminescence kit (Pierce Endogen, IL) and Kodak Biomax MR film (Fisher Scientific, TX). E-Cadherin immunoblots were detected with NBT/BCIP alkaline phosphatase substrate (Pierce Endogen, IL).

Competing interests

The author(s) declare that they have no competing interests.

Authors' contributions

MRH participated in design of the study, carried out the assays, including their quantification and interpretation, and was the primary author of the manuscript. KMW participated in the cell culture, assisted in the assays and their quantification and interpretation, and helped to draft and revise the manuscript. SFD was responsible for the conception of the project, advise and training on experimental design and procedures, aided in the analysis and interpretation of data, and helped revise the manuscript. All authors read and approved the final manuscript.

Acknowledgements

The authors wish to thank Dr. Rebecca Richards-Kortum for critical input during the preparation of this manuscript. This investigation was supported by NIH/NCI CA83957-01A1 and University of Texas Biomedical Engineering Seed Grant to S.D., DOD/US Army BC031906 to M.H, and University of Texas Cooperative Society Awards to KW.

References

1. Levine PH, Steinhorn SC, Ries LG, Aron JL: **Inflammatory breast cancer: the experience of the surveillance, epidemiology, and end results (SEER) program.** *J Natl Cancer Inst* 1985, **74**:291-297.

2. Lopez MJ, Porter KA: **Inflammatory breast cancer.** *Surg Clin North Am* 1996, **76**:411-429.
3. Schmitz AAP, Govek EE, Ötner BB, van Aelst L: **Rho GTPases: signaling, migration, and invasion.** *Exp Cell Res* 2000, **261**:1-12.
4. Hall A, Nobes CD: **Rho GTPases: molecular switches that control the organization and dynamics of the actin cytoskeleton.** *Philos Trans R Soc Lond B Biol Sci* 2000, **355**:965-970.
5. van Golen KL, Davies S, Wu ZF, Wang YF, Bucana CD, Root H, Chandrasekharappa S, Strawderman M, Ethier SP, Merajver SD: **A novel putative low-affinity insulin-like growth factor-binding protein, LIBC (lost in inflammatory breast cancer), and RhoC GTPase correlate with the inflammatory breast cancer phenotype.** *Clin Cancer Res* 1999, **5**:2511-2519.
6. Suwa H, Ohshio G, Imamura T, Wantanabe G, Arii S, Imamura M, Narumiya S, Hiai H, Fukumoto M: **Overexpression of the rhoC gene correlates with progression of ductal adenocarcinoma of the pancreas.** *Br J Cancer* 1998, **77**:147-152.
7. Clark EA, Golub TR, Lander ES, Hynes RO: **Genomic analysis of metastasis reveals an essential role for RhoC.** *Nature* 2000, **406**:532-535.
8. van Golen KL, Bao L, DiVito MM, Wu Z, Prendergrast GC, Merajver SD: **Reversion of RhoC GTPase-induced inflammatory breast cancer phenotype by treatment with a farnesyl transferase inhibitor.** *Mol Cancer Ther* 2002, **1**:575-583.
9. van Golen KL, Wu ZF, Qiao XT, Bao LW, Merajver SD: **RhoC GTPase, a novel transforming oncogene for human mammary epithelial cells that partially recapitulates the inflammatory breast cancer phenotype.** *Cancer Res* 2000, **60**:5832-5838.
10. van Golen KL, Bao LW, Pan Q, Miller FR, Wu ZF, Merajver SD: **Mitogen activated protein kinase pathway is involved in RhoC GTPase induced motility, invasion and angiogenesis in inflammatory breast cancer.** *Clin Exp Metastasis* 2002, **19**:301-311.
11. Tomlinson JS, Alpaugh ML, Barsky SH: **An intact overexpressed E-cadherin/α, β-Catenin axis characterizes the lymphovascular emboli of inflammatory breast carcinoma.** *Cancer Res* 2001, **61**:5231-5241.
12. Alpaugh ML, Tomlinson JS, Kasraeian S, Barsky SH: **Cooperative role of E-cadherin and sialyl-Lewis X/A-deficient MUC1 in the passive dissemination of tumor emboli in inflammatory breast carcinoma.** *Oncogene* 2002, **21**:3631-3643.
13. Alpaugh ML, Tomlinson JS, Shao ZM, Barsky SH: **A novel human xenograft model of inflammatory breast cancer.** *Cancer Res* 1999, **59**:5079-5084.
14. Colpaert CG, Vermeulen PB, Benoy I, Soubry A, van Roy F, van Beest P, Goovaerts G, Dirix LY, van Dam P, Fox SB, Harris AL, van Marck EA: **Inflammatory breast cancer shows angiogenesis with endothelial proliferation rate and strong E-cadherin expression.** *Br J Cancer* 2003, **10**:718-725.
15. Kleer CG, van Golen KL, Braun T, Merajver SD: **Persistent E-cadherin expression in inflammatory breast cancer.** *Mod Pathol* 2001, **14**:458-464.
16. Cavallaro U, Christofori G: **Cell adhesion in tumor invasion and metastasis: loss of the glue is not enough.** *Biochimica et Biophysica Acta* 2001, **1552**:39-45.
17. van Golen KL, Wu ZF, Qiao XT, Bao L, Merajver SD: **RhoC GTPase overexpression modulates induction of angiogenic factors in breast cells.** *Neoplasia* 2000, **2**:418-425.
18. Ethier SP, Kokeny KE, Ridings JW, Dilts CA: **erbB family receptor expression and growth regulation in a newly isolated human breast cancer cell line.** *Cancer Res* 1996, **56**:899-907.
19. Ethier SP: **Human breast cancer cell lines as models of growth regulation and disease progression.** *J Mammary Gland Biol Neoplasia* 1996, **1**:111-121.
20. Sartor CI: **Role of epidermal growth factor receptor and STAT-3 activation in autonomous proliferation of SUM-102PT human breast cancer cells.** *Cancer Res* 1997, **57**:978-987.
21. Maddox AS, Oegema K: **Closing the GAP: A Role for RhoA GAP in Cytokinesis.** *Mol Cell* 2003, **11**:846-848.
22. Klemke RL, Leng J, Molander R, Brooks PC, Vuori K, Cheresh DA: **CAS/Crk coupling serves as a "molecular switch" for induction of cell migration.** *J Cell Biol* 1998, **140**:961-72.
23. Schoenwaelder SM, Burridge K: **Evidence for a calpeptin-sensitive protein-tyrosine phosphatase upstream of the small GTPase Rho. A novel role for the calpain inhibitor calpeptin in the inhibition of protein-tyrosine phosphatases.** *J Biol Chem* 1999, **274**:14359-67.
24. Sward K, Mita M, Wilson DP, Deng JT, Susnjar M, Walsh MP: **The role of RhoA and Rho-associated kinase in vascular smooth muscle contraction.** *Curr Hypertens Rep* 2003, **5**:66-72.
25. Shirakawa K, Wakasugi H, Heike Y, Watanabe I, Yamada S, Saito K, Konishi F: **Vasculogenic mimcry and psuedo-comedo formation in breast cancer.** *Int J Cancer* 2002, **99**:821-828.
26. Shirakawa K, Kobayashi H, Heike Y, Kawamoto S, Brechbiel MW, Kasumi F, Iwanaga T, Konishi F, Terada M, Wakasugi H: **Hemodynamics in vasculogenic mimicry and angiogenesis of inflammatory breast cancer xenograft.** *Cancer Res* 2002, **62**:560-566.
27. Shirakawa K, Tsuda H, Heike Y, Kato K, Asada R, Inomata M, Sasaki H, Kasumi F, Yoshimoto M, Iwanaga T, Konishi F, Terada M, Wakasugi H: **Absence of endothelial cells, central necrosis, and fibrosis are associated with aggressive inflammatory breast cancer.** *Cancer Res* 2001, **61**:445-451.
28. Nobes CD, Hall A: **Rho GTPases control polarity, protrusion, and adhesion during cell movement.** *J Cell Biol* 1999, **144**:1235-1244.
29. Okegawa T, Li Y, Pong RC, Hsieh JT: **Cell adhesion proteins as tumor suppressors.** *J Urol* 2002, **167**:1836-43.
30. Ridley AJ: **Rho GTPases and cell migration.** *J Cell Sci* 2001, **114**:2713-2722.
31. Rottner K, Hall A, Small JV: **Interplay between Rac and Rho in the control of substrate contact dynamics.** *Curr Biol* 1999, **9**:640-648.
32. Kamai T, Tsujii T, Arai K, Takagi K, Asami H, Ito Y, Oshima H: **Significant association of Rho/ROCK pathway with invasion and metastasis of bladder cancer.** *Clin Cancer Res* 2003, **9**:2632-41.
33. Horiuchi A, Imai T, Wang C, Ohira S, Feng Y, Nikaido T, Konishi I: **Up-regulation of small GTPases, RhoA and RhoC, is associated with tumor progression in ovarian carcinoma.** *Lab Invest* 2003, **83**:861-70.
34. Clark EA, Golub TR, Lander ES, Hynes RO: **Genomic analysis of metastasis reveals an essential role for RhoC.** *Nature* 2000, **406**:532-5.
35. Stam JC, Michiels F, van der Kammen RA, Moolenaar WH, Collard JG: **Invasion of T-lymphoma cells: cooperation between Rho family GTPases and lysophospholipid receptor signaling.** *EMBO J* 1998, **17**:4066-4074.
36. Itoh K, Yoshioka K, Akedo H, Uehata M, Ishizaki T, Narumiya S: **An essential part for Rho-associated kinase in the transcellular invasion of tumor cells.** *Nat Med* 1999, **5**:221-225.
37. O'Connor KL, Nguyen BK, Mercurio AM: **RhoA function in lamellae formation and migration is regulated by the alpha6beta4 integrin and cAMP metabolism.** *J Cell Biol* 2000, **148**:253-258.
38. Moorman JP, Luu D, Wickham J, Bobak DA, Hahn CS: **A balance of signaling by Rho family small GTPases RhoA, Rac1, and Cdc42 coordinates cytoskeletal morphology but not cell survival.** *Oncogene* 1999, **18**:47-57.
39. Braga VMM: **Cell-cell adhesion and signalling.** *Curr Opin Cell Biol* 2002, **14**:546-556.
40. Fukata M, Kaibuchi K: **Rho-family GTPases in cadherin-mediated cell-cell adhesion.** *Nat Rev Mol Cell Biol* 2001, **2**:887-897.
41. Vaezi A, Bauer C, Vasioukhin V, Fuchs E: **Actin cable dynamics and Rho/Rock orchestrate a polarized cytoskeletal architecture in the early steps of assembling a stratified epithelium.** *Dev Cell* 2002, **3**:367-381.
42. Hendrix MJC, Softer EA, Meltzer PS, Gardner LMG, Hess AR, Kirschmann DA, Schatteman GC, Seftor REB: **Expression and functional significance of VE-cadherin in aggressive human melanoma cells: Role in vasculogenic mimicry.** *Proc Nat Acd Sci USA* 2001, **98**:8018-8023.

In situ analysis of breast cancer progression in murine models using a macroscopic fluorescence imaging system

Alicia L. Carlson, MS[1#], Michaela R. Hoffmeyer, MA[2#], Kristin M. Wall[1], Paige J. Baugher, PhD[2], Rebecca Richards-Kortum, PhD[1], and Suranganie F. Dharmawardhane, PhD[2*]

Department of Biomedical Engineering[1], Molecular Cell and Developmental Biology Section[2], and Institute for Cellular and Molecular Biology, The University of Texas at Austin, Austin, TX 78712

Running Title: *In situ* image analysis of breast cancer progression

Nonstandard abbreviations: RFP, red fluorescent protein

Keywords: fluorescence imaging, intravital imaging, breast cancer

[#] These authors contributed equally to the manuscript.

[*]To whom correspondence should be addressed:
Department of Anatomy and Cell Biology
Universidad Central del Caribe School of Medicine
P.O. Box 60327
Bayamon, PR 00960-6032
Tel: 512-560-1835, 787-798-3001
E-mail: surangi@mail.utexas.edu, surangi@uccaribe.edu

Acknowledgment of Research Funding:
NSF/Integrative Graduate Education and Research Training Fellowships to M.H. and A.C.
The Department of Defense /BCRP Pre-Doctoral Fellowship #BC031906 to M.H.
NIH/National Institute of Cancer Research R01CA103830 to R.R.K
The Department of Defense/BCRP #DAMD17-02-1-0582,
American Institute of Cancer Research 03-31-06, and Whitaker Foundation/UT Austin Biomedical Engineering Department Seed Grant to S.D.

ABSRACT

Background and Objective: The goal of this study was to use an inexpensive macroscopic imaging system to monitor fluorescently-tagged tumor progression in mouse models in real-time with minimal intervention.

Study Design/Materials and Methods: This system is illuminated from a Xenon arc lamp and uses a fiber optic probe to deliver white light or excitation wavelengths via specific bandpass filters. Fluorescence emission from SCID and nude mice following mammary fat pad injection of red fluorescence protein (RFP)-expressing human breast cancer cell lines was recorded and quantified using a SLR digital camera.

Results: This simple system enabled the verification of successful tumor take and temporal quantification of tumor progression in mouse models.

Conclusion: The macroscopic fluorescence imaging system represents an inexpensive and portable tool to facilitate non-invasive *in situ* cancer detection with the potential to monitor fluorescent tumor formation. This system is also useful for identification of distant metastases and investigation of the efficacy of potential cancer preventatives and therapeutics.

INTRODUCTION

Breast cancer is estimated to account for 32% of the new cancer cases in woman in 2005 and is the second major cause of cancer deaths behind lung cancer. Metastatic spread of breast cancer complicates treatment and lowers patient prognosis drastically [1]. Use of mouse models is a common and effective research tool to study breast cancer progression, potential oncogenes and tumor suppressors, and to investigate prospective therapeutics to specifically target metastatic spread [2-5]. Conventional methods for studying cancer progression and therapeutic agent efficacy include end point analysis of metastases following primary mammary tumor induction in mouse models. Such end point analysis limits investigation of the individual steps in the multi-facetted process of metastasis. Therefore, a more recent approach has been to develop novel *in situ* imaging modalities to facilitate these needs [6-28].

Analyzing tumor progression via classic methods of experimental metastasis in mouse models has many limitations. Specifically, mouse mammary fat pad injection does not always lead to 100 percent successful mammary tumor establishment. Post-injection observation for successful tumor establishment requires examination of the injection site for growth over several weeks. Scar tissue formation at the site of injection often obscures successful tumor take. Furthermore, identification of potential metastatic sites for further histological examination is difficult for those not trained in pathology and often must occur after mouse sacrifice. Therefore, our goal was to adapt a macroscopic imaging system to verify successful mammary fat pad tumor implantation, monitor tumor growth over time, and reliably delineate metastatic sites for detailed histological examination.

Herein, we describe a preliminary study using an inexpensive *in vivo* macroscopic imaging system for real-time image analysis of tumor formation by red fluorescent protein (RFP) expressing breast cancer cells in mice. This system uses a fiber optic probe to deliver excitation light to the mouse in order to verify successful mammary fat pad tumor take and temporally monitor tumor progression via fluorescence intensity. Additionally, this system can be employed to locate small metastatic lesions via

fluorescent signal non-invasively or by minimal invasion using a skin flap. Fluorescent protein emission can also be used by this system to identify potential metastatic areas of interest for further histological analysis. The macroscopic fluorescence imaging system thus represents an inexpensive and portable tool to facilitate *in situ* cancer detection without the need to anesthetize the animal.

MATERIALS AND METHODS

Cell Culture

The SUM 149 inflammatory breast cancer (IBC) cell line used for the study was developed from pleural effusions of breast cancer patients [29,30] and was a generous gift of Dr. Stephen Ethier, The University of Michigan, MI. SUM 149 cells were cultured in F-12 Hams medium (Gibco^{TM}, CA) supplemented with 5% fetal bovine serum (Tissue Culture Biologicals, CA), insulin, and hydrocortisone and cultured in a humidified 5% CO_2 atmosphere at 37°C. The human breast cancer cell line MDA-MB-435α6HG6 was selected according to α6 expression and metastatic efficiency in the nude mouse model as described in [31] and was the kind gift of Dr. Janet E. Price, MD Anderson Cancer Center, Houston, TX. MDA-MB-435α6HG6 cells were cultured in Dulbecco's modified Eagle's medium (DMEM) (Gibco^{TM}, CA) with 10% fetal bovine serum (Tissue Culture Biologicals, CA) and cultured in a humidified 5% CO_2 atmosphere at 37°C.

Vector Construction

SUM 149 cells were transfected with pIRESneo2 DsRed2 (RFP) and the MDA-MB-435 α6HG6 cells were transfected with pIRESpuro3 DsRed2 (RFP) using Lipofectamine as per the manufacture's protocol (Invitrogen, CA). RFP-SUM 149 cells were selected in neomycin and RFP-MDA-MB-435-α6HG6 cells were selected in puromycin. The MDA-MB-435α6HG6 cells stably expressing RFP were further selected via flow cytometry. RFP expression of both cell lines remained stable at ~99%

expression in cells that were maintained for two to three months in cell culture and ~95% in cell lines that were restarted following storage in liquid nitrogen for at least a year.

Macroscopic Imaging System

A schematic of the macroscopic imaging system is shown in Figure 1. Light from a 300W Xenon arc lamp with an integrated parabolic reflector (Perkin Elmer, CA) was directed by a cold mirror to the excitation filter wheel (Oriel Instruments, CT). The cold mirror rejected radiation below 300 nm and above 625 nm, preventing ultraviolet and infrared radiation from reaching the excitation filter. A bandpass filter centered at 545 nm was used to select the desired excitation wavelengths (HQ545/30x, Chroma Technology, VT). One filter slot remained open for white light illumination to visualize the position of the mouse. Excitation light was focused onto a flexible fiber optic light guide 5 mm in diameter and 2.5 m long (Multimode Fiber Optics Inc., NJ) for delivery to the mouse. With the 545 nm excitation filter in place, approximately 60 mW of light exited the light guide and diverged rapidly to illuminate a large region of the mouse. Fluorescence emission from the mouse was recorded using a Canon EOS-D30 digital camera equipped with two emission filters, a bandpass filter centered at 610nm (HQ610/75m, Chroma Technology, VT) and a 570nm longpass filter (Schott OG570, Newport Industrial Glass, Inc., CA), attached prior to the camera lens. The filters were easily removed for imaging with white light illumination.

***In vivo* imaging of RFP-expressing cells**

All mouse experiments were approved by and preformed in accordance with the Institutional Animal Care and Use Committee (IACUC) at The University of Texas at Austin. For *in vivo* imaging of RFP-SUM 149 breast cancer progression, $1x10^6$ cells suspended in PBS were injected into the mammary fat pad of 6 week old female SCID (severe combined immunodeficiency) mice (CBySmn.CB17-*Prkdc*^{scid}/J , Charles Rivers, MA). For RFP-MDA-MB-435α6HG6 *in vivo* imaging experiments, $2x10^6$

cells suspended in PBS were injected into the mammary fat pad of 6 week old female nude immunocompromised mice (*nu/nu,* Charles Rivers, MA). Mice were manually restrained and imaged under white light illumination. After fitting the camera with the emission filter, the mice were imaged under RFP excitation light. Imaging occurred 2-3 times per week. Digital images were checked for saturation in each color channel and those that were not saturated were then converted to grayscale using Matlab (The MathWorks, Natick, MA). Image intensity was normalized by the camera exposure time prior to analysis. Tumor area was manually traced in each grayscale image using Image J software (freeware provided by the NIH, Bethesda, MD). The mean grayscale value was calculated and the number of pixels was determined and converted to mm^2 for the traced tumor area and plotted versus time.

RESULTS

To verify the expression of RFP and the lack of fluorescence in the parental, non-RFP breast cancer cells, we viewed cell pellets containing $4x10^6$ cells with the macroscopic imaging system prior to mammary fat pad injection (Fig. 2A and B). All of the RFP-tagged breast cancer cells that were used for this study expressed RFP at a 99-100% efficiency. Figure 2A illustrates cell pellets viewed under RFP excitation for SUM 149 (Fig. 2A left) and RFP-tagged SUM 149 (Fig. 2A right) cells. MDA-MB-435α6HG6 cells were also pelleted (Fig. 2B left) and imaged along side a RFP-tagged MDA-MB-435α6HG6 cell pellet (Fig. 2B right). No fluorescent signal was detected under RFP excitation by our system for either of the parental, non-RFP expressing cell lines. RFP and parental MDA-MB-435α6HG6 cells were also imaged by fluorescence microscopy (Fig. 2C-F). Again, no RFP fluorescence was detected under 100x magnification from the parental cell line (Fig. 2D) while the RFP-tagged MDA-MB-435α6HG6 cells exhibited uniform red fluorescence at a 100% efficiency (Fig. 2F). The fluorescent imaging system was easily able to detect $1X10^5$ of these RFP-tagged breast cancer cells in the syringe prior to

injection and underneath the mouse skin following injection at six times more fluorescence intensity than background autofluorescence (Fig. 2 G, H).

Figure 3 represents white light and fluorescent images of stably expressing RFP-SUM 149 IBC human breast cancer establishment and progression in the mammary fat pad of female SCID mice. White light images represent the location and relative size of the mammary tumor. Nodules, such as the one observed in the white light image at three days after mammary fat pad injection, may represent scar tissue or inflammation rather than an actual tumor. Using our macroscopic fluorescence imaging system to excite RFP fluorescence, we were able to visualize the site of breast cancer cell injection in the mammary fat pad and tumor take and survival in the SCID mouse host staring from time of injection. At day 3, the tumor was evident in the fluorescence image thus, indicating successful mammary tumor establishment. At day 35, the same tumor showed a substantial increase in red fluorescence signal and the corresponding white light image showed a clearly discernable mammary tumor.

In parallel, female SCID mice were also injected in the mammary fat pad with non-RFP expressing SUM 149 human breast cancer cells. Two days post injection, a region of potential mammary tumor formation by the injected non-fluorescent breast cancer cells was perceived in the white light image and, as expected, there was no detectable fluorescence signal under RFP excitation illumination. By day 34, a non-RFP expressing SUM 149 tumor was clearly visible under white light in the mammary fat pad of the SCID mouse. As expected, no RFP emission was detected under fluorescence imaging. Interestingly, the tumor exhibited diminished background fluorescence with time. This was possibly due to the displacement of fluorescent connective tissue components, such as collagen, by the growing tumor within the mouse.

Using the macroscopic fluorescence imaging system, we monitored RFP-tagged SUM 149 mammary tumor growth in SCID mice over time by analyzing changes in tumor fluorescence intensity. Fluorescent images of the RFP-tagged SUM 149 tumors were converted to grayscale and the fluorescent

tumor area traced. Mean grayscale pixel value within the traced tumor area was plotted for each image. An increase in fluorescence intensity was evident with increased mammary tumor size. A small, initial decrease in fluorescence intensity was observed near day 6. This is possibly due to the death of some of the injected RFP expressing cancer cells that did not successfully take within the mammary tissue. After this initial decrease, the fluorescent intensity steadily increased as the RFP-tagged tumor grew in size. The autofluorescence from the non-RFP expressing tumor was substantially low compared to the RFP-tagged tumor (Fig. 4A).

In addition to measuring the increase in fluorescence intensity, the size of the RFP-tagged SUM 149 mammary tumor over time was also determined by analyzing the number of pixels within the detectable RFP signal in the fluorescence images. The area in pixels^2, as determined using the Image J software, was converted to mm^2 and plotted versus time. This analysis demonstrates a slight decrease in area of the fluorescence region at day 6, corresponding to the decrease in fluorescence intensity and the expected death of some of the injected RFP expressing cancer cells that did not successfully take within the mammary tissue. Beyond day 6, the size of the tumor increased as a function of time, exhibiting exponential growth after ~ day 35 (Fig. 4B).

Tumor growth was also determined for both RFP-tagged and non-RFP-expressing tumors by a more conventional method, using caliper measurements. The fluorescence imaging system clearly detected RFP-SUM 149 cells from day 0. However, the tumor size could not be determined by caliper measurements until day 30 when the tumors reached a mean area of 3x3 mm^2, illustrating the utility of the imaging system for early tumor detection. These data also demonstrate that the low fluorescence in the non-RFP tumor was not due to a decrease in tumor size because at 48 days following inoculation, the RFP-tagged tumor was 5.75 x 5.2 mm^2 in size while the non-RFP expressing tumor measured at 6.4 x 5.8 mm^2 (Fig. 4C).

Here, we have demonstrated that the macroscopic imaging system enabled a direct analysis of tumor growth over time by monitoring the increase in fluorescence signal. We also demonstrated that the RFP-expressing SUM 149 cell line successfully maintained fluorescence in a mouse over an extended period of time. Non-RFP expressing SUM 149 mammary tumors showed no increase in fluorescence signal as the tumor increased in size over time, as expected. The low background fluorescence measured was autofluorescence signal from the skin and hair of the SCID mouse. Interestingly, a modest decrease in autofluorescence intensity was seen in the non-RFP SUM 149 tumor. This may have been due to the displacement of fluorescent connective tissue components that contribute to the autofluorescence of SCID mouse skin or host-formed fibrous protein encapsulation of the tumor.

A similar set of experiments was preformed using a highly metastatic RFP-tagged human breast cancer cell line in a different immunocompromised mouse strain to illustrate the versatility of our system. Figure 5 presents white light and fluorescent images of stably expressing RFP-MDA-MB-435α6HG6 human breast tumors in the mammary fat pad of female athymic, nude mice. In the day 7 fluorescent image, RFP emission was obvious at the site of injection, indicating successful MDA-MB-435α6HG6 tumor cell take and survival in the nude mouse host. At day 71, the white light image of the same mouse showed a clearly discernable mammary tumor. The image of this tumor under RFP excitation on day 71 showed a substantial increase in fluorescence signal. In parallel, female nude mice were also injected in the mammary fat pad with non-RFP expressing MDA-MB-435α6HG6 human breast cancer cells which emitted no fluorescence above background autofluorescence of the skin.

We monitored RFP-tagged MDA-MB-435α6HG6 mammary tumor growth in nude mice over time by analyzing increases in tumor fluorescence intensity. As demonstrated in Figure 6, an increase in fluorescence intensity was evident with increased mammary tumor size. Therefore, the macroscopic

fluorescence imaging system can be used conveniently to non-invasively quantify fluorescent tumor progression of a metastatic breast cancer cell line.

Figure 7 presents images of distant fluorescent metastases. We were able to detect areas of distant metastases by whole-body imaging; however, intravital imaging where a skin flap is opened over the areas of interest, as described in [14], is necessary for a complete analysis of metastatic lesions by our system in the current configuration. Following necropsy, red fluorescence signal from distant lung metastases was easily detected by our system. This verified the existence of metastatic lesions, since such lesions were not obvious to the untrained, naked eye. Therefore our system can be easily used to detect and quantify metastases without prior histopathology.

DISCUSSION

Here in, we have detailed the utilization of a macroscopic fluorescence imaging system to monitor RFP-tagged human tumor progression in immunocompromised mice in real-time with no or minimal intervention. Using this system, we can determine if RFP-expressing human breast cancer cells have successfully established a mammary tumor in the mouse at a much earlier time than visualizing tumor growth at approximately 1-2 weeks post-injection as a means to verify successful implantation. Furthermore, such methodology can be used to monitor tumor growth over time by measuring an increase in fluorescence intensity from the RFP-tagged tumor. Finally, this system can successfully locate the fluorescence signal from metastatic tumors and thus facilitate identification of regions of interest for further examination by histopathology.

The development and optimization of this system was not without complication. The mouse chow (Harlan Teklab, IN) was found to fluoresce under excitation for RFP and can be seen in the intestinal tract of many of the mouse images (data not shown). While this did not hinder analysis of tumor take and

tumor growth over time, this can easily be reduced by feeding mice corn-based chow devoid of the chlorophyll responsible for this background fluorescence. Also, we found it necessary to use the SCID mouse for RFP-SUM 149 experiments because we had limited success establishing tumors with this cell line in nude mice. To avoid the strong fluorescence signal of the hair of the SCID mice, we shaved them prior to imaging. However, even with this complication, we could still successfully detect tumor take and monitor tumor growth over time. With the highly metastatic human breast cancer cell line RFP-MDA-MB-435α6HG6, we could utilize nude mice and successfully monitored tumor take and progression with results similar to those obtained with the RFP-SUM 149 tumors in SCID mice. Therefore, we believe this system can be successfully employed with many different mouse strains.

So far, few studies have utilized RFP to image cancer and these studies have used surgical orthotopic implantation (SOI) to transplant fragments of RFP-tagged tumors into rodent models [18]. In this study, we describe the use of RFP-tagged cells to establish mammary tumors in mouse models. We used DsRed as the fluorescent tag in these studies because this protein can be excited by 488 nm argon lasers and fluoresces outside the range of autofluorescence of media, glassware and cellular components, thus resulting in higher signal to noise ratios. Moreover, since DsRed fluoresces at a longer wavelength than other autofluorescent proteins, the tissues should absorb less energy at this wavelength. The sensitivity of our system to detect a minimum of $1x10^5$ RFP-tagged cells *in situ* was moderate at 6-7 times over the autofluorescence signal, but this may be improved by the use of GFP tags as previously described [6-23] or improved RFP constructs.

An interesting and unexpected result of this study was a decrease in background fluorescence over time from the non-RFP mouse tumor. In mice, host response to tumor growth can result in the formation of a fibrous tissue cap surrounding established tumors [3, 32-34]. The observed decrease in fluorescence

could be a result of fibrous cap formation or possibly from displacement of autofluorescent skin and connective tissue components as the tumor grew in size.

Imaging of optically-tagged cancer cells in mice has been successfully utilized to study the growth and metastatic spread of a variety of cancers and to test the efficacy of potential chemotherapies [6-28]. Hoffman *et al*. employs a light box system with fiber optic probe delivery of blue light for low resolution, whole body imaging of SOI GFP and RFP tagged-tumors in mice. This system is similar to our own but employs a cooled charge-coupled device (CCD) camera for detection [6-19]. The *in vivo* bioluminescence imaging system developed by Contag *et al*. detects light emitted from bioluminescent cells within mice with a CCD camera. Bioluminescent imaging has been utilized to detect cancer cells from the time of inoculation through tumor progression and to evaluate cancer therapies [24-28]. Image analysis of bioluminescently-tagged tumor cells usually involves more manipulation than analysis of fluorescent cells. In order to bioluminesce, the cells need access to oxygen to be metabolically active and require external luciferin as a substrate unless engineered to produce it *in situ* [25]. Furthermore, some of the previously mentioned intravital imaging modalities also require anesthetization of the animal and are invasive, requiring a skin flap opening in the animal [14, 16, 17, 21-24]. Our system enabled noninvasive examination of breast cancer progression *in vivo* without the need for anesthetization or surgery.

Finally, the macroscopic fluorescence imaging system described herein is inexpensive and easy to assemble. We utilized a consumer-grade digital SLR camera to obtain images which can be purchased for less than $800. Although we used a filtered arc lamp as a source of excitation, several inexpensive alternatives could be used. For example, excitation light can be provided by a Helium Neon laser, a diode pumped solid state (DPSS) laser, or a Light Emitting Diode (LED). HeNe and DPSS lasers provide very narrow linewidth excitation. For lower powers, a HeNe laser costs as little as $500 (Melles Griot) and a DPSS laser can be purchased for as little at $800 (Midwest Laser). Recently, a blue LED flashlight was

used as an inexpensive alternative for whole-body imaging of GFP- or RFP-tagged tumors in nude mice [19]. An LED, yielding 60 mW of power, with driver and necessary accessories costs approximately $80 (TheLEDLight.com). The total cost of our system was under $4000, including the camera. However, if a LED is used as the excitation source rather than the arc lamp, the cost of the system decreases to under $1850, making this a very inexpensive intravital imaging modality.

Clearly, the mouse model of breast cancer in conjunction with advances in intravital imaging affords many advantages over traditional *in vitro* and *in vivo* assays in the study of metastatic breast cancer progression. Intravital imaging can be performed with simple tools, and affords the ability to follow tumor progression over time in a single animal. Thus, studies can be carried out with fewer animals reducing artifacts due to biological variability. This macroscopic imaging system will be used in future applications to investigate the efficacy of potential anti-cancer preventatives and therapies.

ACKNOWLEDGEMENTS

We wish to thank Vivian Mack for expert technical assistance and Dr. Janet Price (MD Anderson cancer Center, Houston, TX) and Dr. Stephen Ethier (University of Michigan, MI) for providing the breast cancer cell lines.

References

1. Jemal A, Murray T, Ward E, Samuels A, Tiwari RC, Ghafoor A, Feuer EJ, and Thun MJ. Cancer Statistics, 2005. CA Cancer J Clin 2005; 55:10-30.

2. Killion JJ, Radinsky R, and Fidler IJ. Orthotopic models are necessary to predict therapy of transplantable tumors in mice. Cancer Metastasis Rev 1999; 17: 279-284.

3. Price JE. Analyzing the metastatic phenotype. J Cell Biochem 1994; 56: 16-22.

4. Price JE. Metastasis from human breast cancer cell lines. Breast Cancer Res Treat 1996; 39: 93-102.

5. Price JE, and Zhang RD. Studies of human breast cancer metastasis using nude mice. Cancer Metastasis Rev 1990; 8: 285-297.

6. Chishima T, Miyagi Y, Wang X, Yamaoka H, Shimada H, Moosa AR, and Hoffman RM. Cancer invasion and micrometastasis visualized in live tissue by green fluorescent protein expression. Cancer Res 1997; 57: 2042-2047.

7. Yang M, Baranov E, Jiang P, Sun FX, Li XM, Li L, Hasegawa S, Bouvet M, Al-Tuwaijri M, Chishima T, Shimada H, Moossa AR, Penman S, and Hoffman RM. Whole-body optical imaging of green fluorescent protein-expressing tumors and metastases. Proc Natl Acad Sci U S A 2000; 97: 1206-1211.

8. Yang M, Baranov E, Moossa AR, Penman S, and Hoffman RM. Visualizing gene expression by whole-body fluorescence imaging. Proc Natl Acad Sci USA 2000; 97: 12278-12282.

9. Rashidi B, Yang M, Jiang P, Baranov E, An Z, Wang X, Moossa AR, and Hoffmam RM. A highly metastatic Lewis lung carcinoma orthotopic green fluorescent protein model. Clin Exp Metastasis 2000; 18: 57-60.

10. Hoffman RM. Orthotopic metastatic mouse models for anticancer drug discovery and evaluation: a bridge to the clinic. Invest New Drugs 2000; 17: 343-359.

11. Yang M, Baranov E, Moossa AR, Penman S, and Hoffman RM. Visualizing gene expression by whole-body fluorescence imaging. Proc Natl Acad Sci USA 2000; 97: 12278-12282.

12. Zhao M, Yang M, Baranova E, Wang X, Penman S, Moossa AR, and Hoffman RM. Spatial-temporal imaging of bacterial infection and antibiotic response in intact animals. Proc Natl Acad Sci USA 2001; 98: 9814-9818.

13. Yang M, Baranov E, Li XM, Wang JW, Jiang P, Li L, Moossa AR, Penman S, and Hoffman RM. Whole-body and intravital optical imaging of angiogenesis in orthopically implanted tumors. Proc Natl Acad Sci USA 2001; 98: 2616-2621.

14. Yang M, Baranov E, Wang JW, Jiang P, Wang X, Sun FX, Bouvet M, Moossa AR, Penman S, and Hoffman RM. Direct external imaging of nascent cancer, tumor progression, angiogenesis, and

metastasis on internal organs in the fluorescent orthotopic model. Proc Natl Acad Sci USA 2002; 99: 3824–3829.

15. Schmitt CA, Fridman JS, Yang M, Baranov E, Hoffman RM, and Lowe SW. Dissecting p53 tumor suppressor function in vivo. Cancer Cell 2002; 1: 289-298.

16. Yamamoto N, Yang M, Jiang P, Tsuchiya H, Tomita K, Moossa AR, and Hoffman RM. Real-time GFP imaging of spontaneous HT-1080 fibrosarcoma lung metastases. Clin Exp Metastasis 2003; 20: 181–185.

17. Amoh Y, Li L, Yang M, Jiang P, Moossa AR, Katsuoka K, and Hoffman RM. Hair follicle-derived blood vessels vascularize tumors in skin and are inhibited by Doxorubicin. Cancer Res 2005; 65: 2337-2343.

18. Hoffman RM. Orthotopic metastatic (MetaMouse) models for discovery and development of novel chemotherapy. Methods Mol Med. 2005;111:297-322.

19. Yang M, Luiken G, Baranov E, and Hoffman RM. Facile whole-body imaging of internal fluorescent tumors in mice with an LED flashlight. BioTechniques 2005; 39:170-172.

20. Wyckoff JB, Jones JG, Condeelis JS, and Segall JE. A critical step in metastasis: i*n vivo* analysis of intravasation at the primary tumor. Cancer Res 2000; 60: 2504-2511.

21. Wang W, Wyckoff JB, Frohlich VC, Oleynikov Y, Huttelmaier S, Zavadil J, Cermak L, Bottinger EP, Singer RH, White JG, Segall JE, and Condeelis JS. Single cell behavior in metastatic primary mammary tumors correlated with gene expression patterns revealed by molecular profiling. Cancer Res 2002; 62: 6278-6288.

22. Ahmed F, Wyckoff J, Lin EY, Wang W, Wang Y, Hennighausen L, Miyazaki JI, Jones J, Pollard JW, Condeelis JS, and Segall JE. GFP expression in the mammary gland for imaging of mammary tumor cells in transgenic mice. Cancer Res 2002; 62: 7166–7169.

23. Wyckoff JB, Wang W, Lin EY, Wang Y, Pixley F, Stanley ER, Graf T, Pollard JW, Segall JE, and Condeelis JS. A paracrine loop between tumor cells and macrophages is required for tumor cell migration in mammary tumors. Cancer Res 2004; 64: 7022-7029.

24. Edinger M, Sweeney TJ, Tucker AA, Olomu AB, Negrin RS, Contag CH.. Noninvasive assessment of tumor cell proliferation in animal models. Neoplasia 1999; 4: 303-310.

25. Rehemtulla A, Stegman LD, Cardozo SJ, Gupta S, Hall DE, Contag CH, and Ross BD. Rapid and quantitative assessment of cancer treatment response using in vivo bioluminescence imaging. Neoplasia 2000; 2: 491-495.

26. Edinger M, Cao YA, Verneris MR, Bachmann MH, Contag CH, and Negrin RS. Revealing lymphoma growth and the efficacy of immune cell therapies using in vivo bioluminescence imaging. Blood 2003; 101: 640-648.

27. Mandl SJ, Mari C, Edinger M, Negrin RS, Tait JF, Contag CH, and Blankenberg FG. Multi-modality imaging identifies key times for Annexin V imaging as an early predictor of therapeutic outcome. Mol Imaging 2004; 3: 1-8.

28. Doyle TC, Burns SM, and Contag CH. *In vivo* bioluminescence imaging for integrated studies of infection. Cell Microbio 2004; 6: 303-317.

29. Ethier SP, Kokeny KE, Ridings JW, and Dilts CA. erbB family receptor expression and growth regulation in a newly isolated human breast cancer cell line. Cancer Res 1996; 56: 899-907.

30. Ethier SP. Human breast cancer cell lines as models of growth regulation and disease progression. J Mammary Gland Biol Neoplasia 1996; 1: 111-121.

31. Mukhopadhyay R, Theriault RL, and Price JE. Increased levels of alpha6 integrins are associated with the metastatic phenotype of human breast cancer cells. Cell Exp Metastasis 1999; 17: 325-332.

32. Astoul P, Colt HG, Wang X, Boutin C, and Hoffman RM. "Patient-like" nude mouse metastatic model of advanced human pleural cancer. J Cell Biochem 1994; 56: 9-15.

33. Kubota T. Metastatic models of human cancer xenografted in the nude mouse: The importance of orthotopic transplantation. J Cell Biochem 1994; 56: 4-8.

34. Lacy AA, Collier T, Price JE, Dharmawardhane S, and Richards-Kortum R. Near real-time in vivo confocal imaging of mouse mammary tumors. Front Biosci 2002; 7:1-7.

Figure Legends

Figure 1. Schematic of macroscopic fluorescence imaging system. Light from a Xenon arc lamp is directed by mirror to the excitation filter wheel with a bandpass filter centered at 545 nm. Excitation light enters a flexible fiber optic light guide for delivery to the mouse. Fluorescence emission from the mouse is recorded using a digital camera fitted with two emission filters, a bandpass filter centered at 610 nm and a 570 nm longpass filter.

Figure 2. Verification of red fluorescence of human breast cancer cells stably expressing RFP. **A,** Fluorescence images of cell pellets ($4x10^6$ cells) of non-RFP (left tube) or RFP-tagged (right tube) SUM 149 cells taken with the macroscopic imaging system. **B**, Fluorescence images of cell pellets ($4x10^6$) of non-RFP (left tube) and RFP-tagged (right tube) MDA-MB-435α6HG6 cells. **C,** Bright field micrograph at 100x magnification. **D,** Fluorescence micrograph of non-RFP MDA-MB-435α6HG6 cells. **E**, Bright field micrograph at 100x magnification. **F**, Fluorescence micrograph of RFP-tagged MDA-MB-435α6HG6 cells. **G**, Fluorescence images of RFP-tagged MDA-MB-435α6HG6 cells in syringe during injection into mammary fat pad of nude mouse. **H**, Fluorescence images of RFP-tagged MDA-MB-435α6HG6 cells underneath nude mouse skin immediately following mammary fat pad injection.

Figure 3. Images of RFP- or non-RFP- expressing SUM 149 mammary tumors in female SCID mice. A, Tumors created from RFP-tagged SUM-149 cells. Top row, images under white light; bottom row, images at 580nm. Left column, 3 days; right column, 35 days following injection. **B**, Tumors created from non-RFP SUM 149 cells. Top row, images under white light; bottom row, images at 580nm excitation. Left column, 2 days; right column, 34 days following injection. Arrows indicate tumor site.

Figure 4. Fluorescence intensity and area of RFP- or Non-RFP- expressing SUM 149 mammary tumors in SCID mice as a function of time. A, SCID mice with RFP and non-RFP tagged SUM 149 mammary tumors were imaged under RFP excitation using the macroscopic imaging system. Images were converted to grayscale and mean grayscale pixel value from the traced tumor area was plotted versus time. **B**, Area of the RFP-tagged SUM 149 mammary tumor was measured from the fluorescence images and converted to mm^2. The tumor area is plotted versus time. **C**, The areas of same RFP and non-RFP tagged SUM 149 mammary tumors were measured using calipers starting at day 30 following injection when the tumors were quantifiable by caliper measurements.

Figure 5. Images of RFP- or non-RFP-expressing MDA-MB-435α6HG6 mammary tumors in female athymic, nude mice. Left column, images under white light; right column, images at 580nm. Top row, non-RFP-tagged MDA-MB-435α6HG6 mammary tumors. Middle row, RFP-tagged MDA-MB-435α6HG6 mammary tumor at day 7, post-mammary cancer cell injection. Bottom row, RFP-tagged MDA-MB-435α6HG6 mammary tumor at day 71.

Figure 6. Fluorescence intensity RFP- or non-RFP-expressing MDA-MB-435α6HG6 mammary tumors in nude mice as a function of time. RFP- or non-RFP-expressing MDA-MB-435α6HG6 cells were injected into the mammary fat pads of two female athymic, nude mice. Tumor growth was monitored via fluorescent image analysis using the macroscopic imaging system. Images were converted to grayscale and the mean grayscale pixel value for the traced tumor area was plotted versus time.

Figure 7. Images of lung metastases from RFP-tagged MDA-MB-435α6HG6 mammary tumors. RFP- tagged MDA-MB-435α6HG6 human breast cancer cells were injected into the mammary fat pad of

female, nude athymic mice. The mammary tumor was allowed to grow for 71 days. Left column, images under white light; right column, images at 580nm. Top row, mouse with open chest cavity. Bottom row, excised lung with metastases seen as white nodules (black arrows) under white light and RFP expressing metastatic lesions verified by fluorescent imaging at 580 nm (white arrows).

Fig. 1, Carlson, et al.

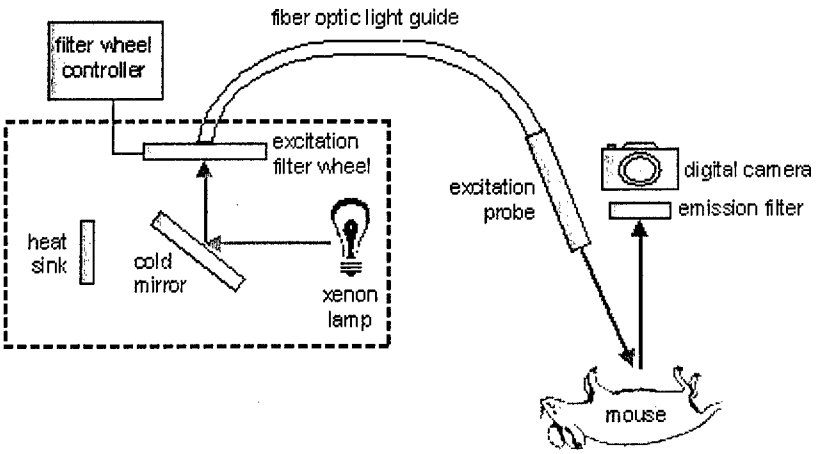

Fig. 2, Carlson, et al.

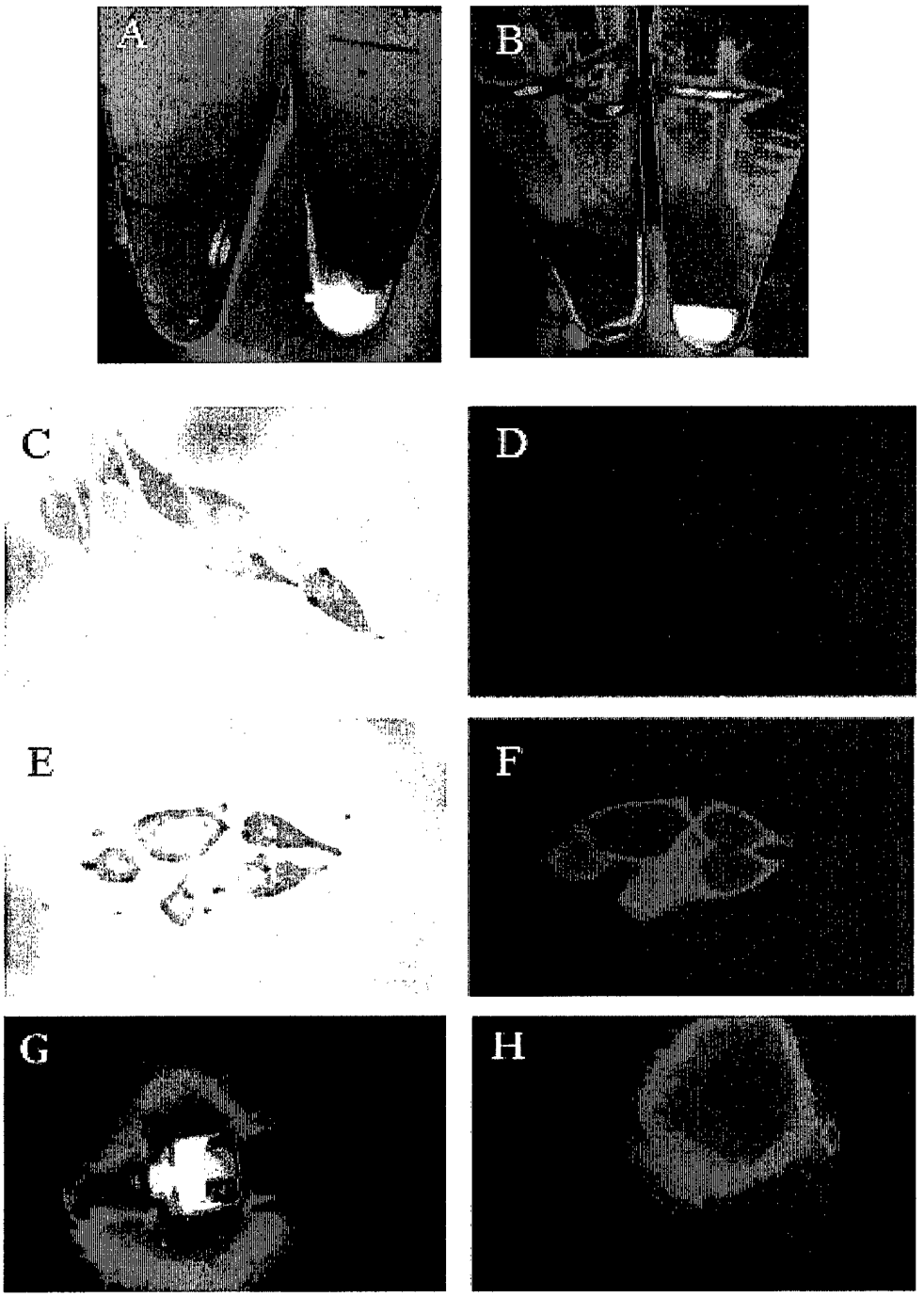

Fig. 3, Carlson, et al.

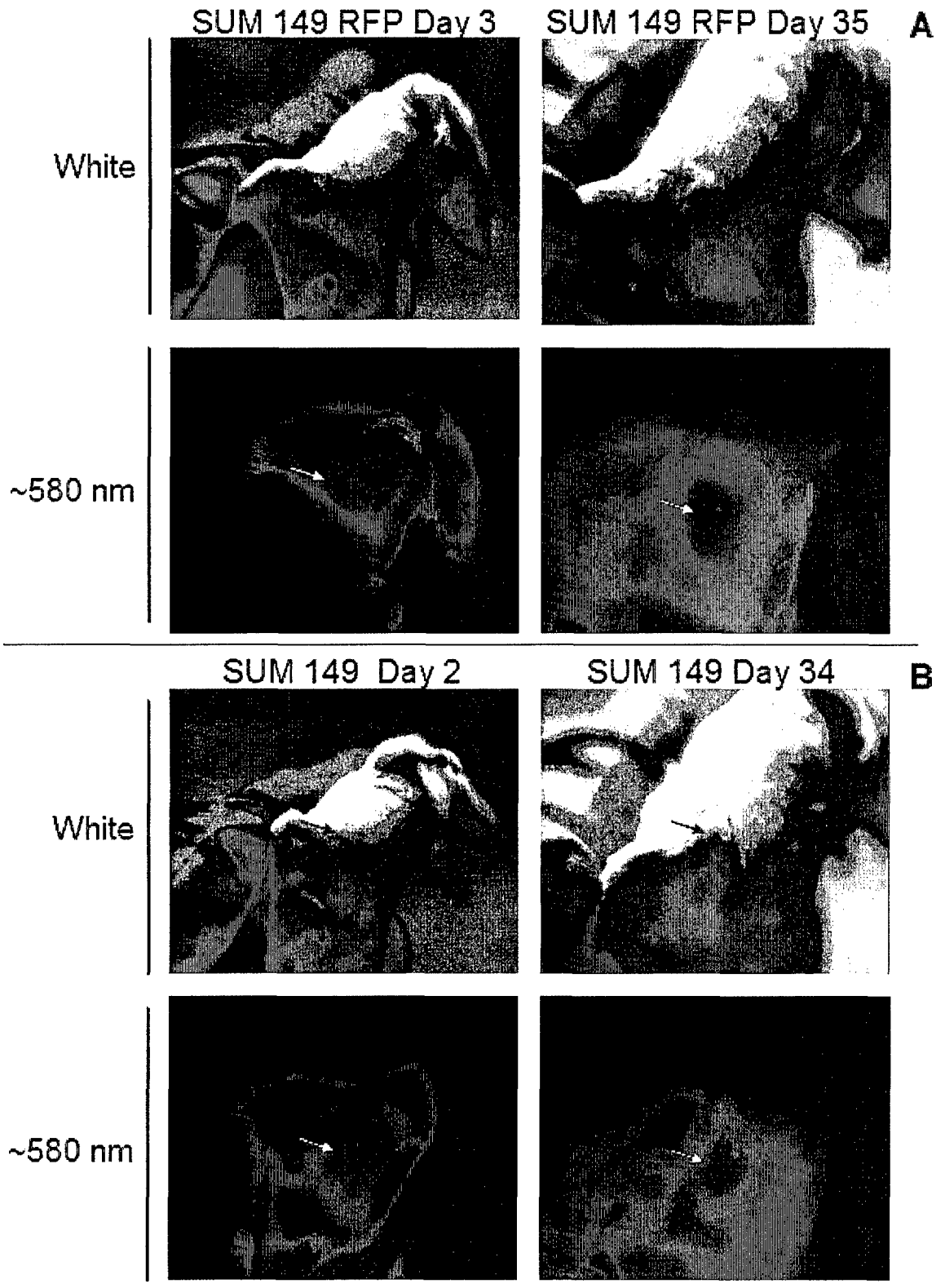

Fig. 4, Carlson, et al.

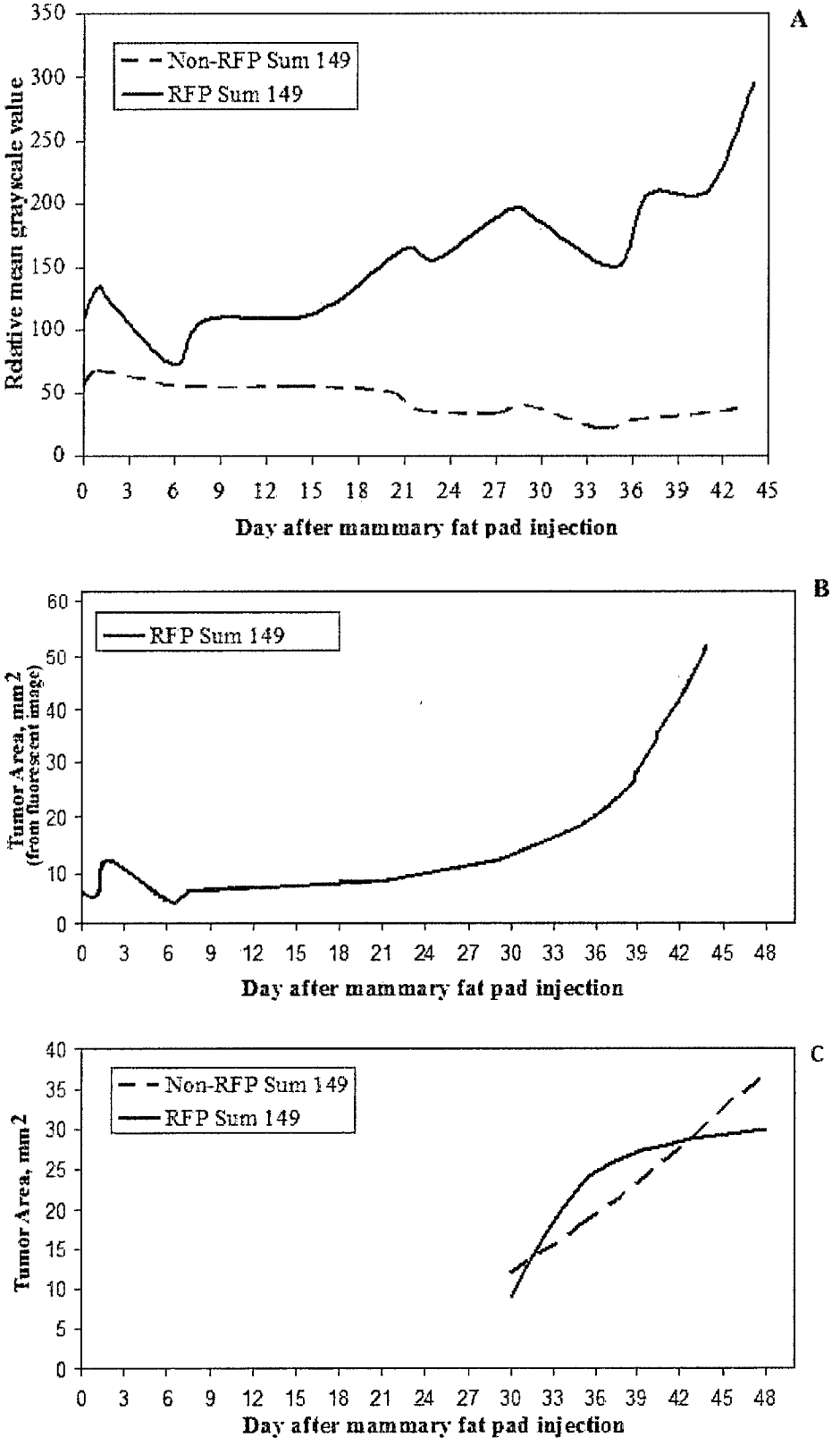

Fig. 5, Carlson, et al.

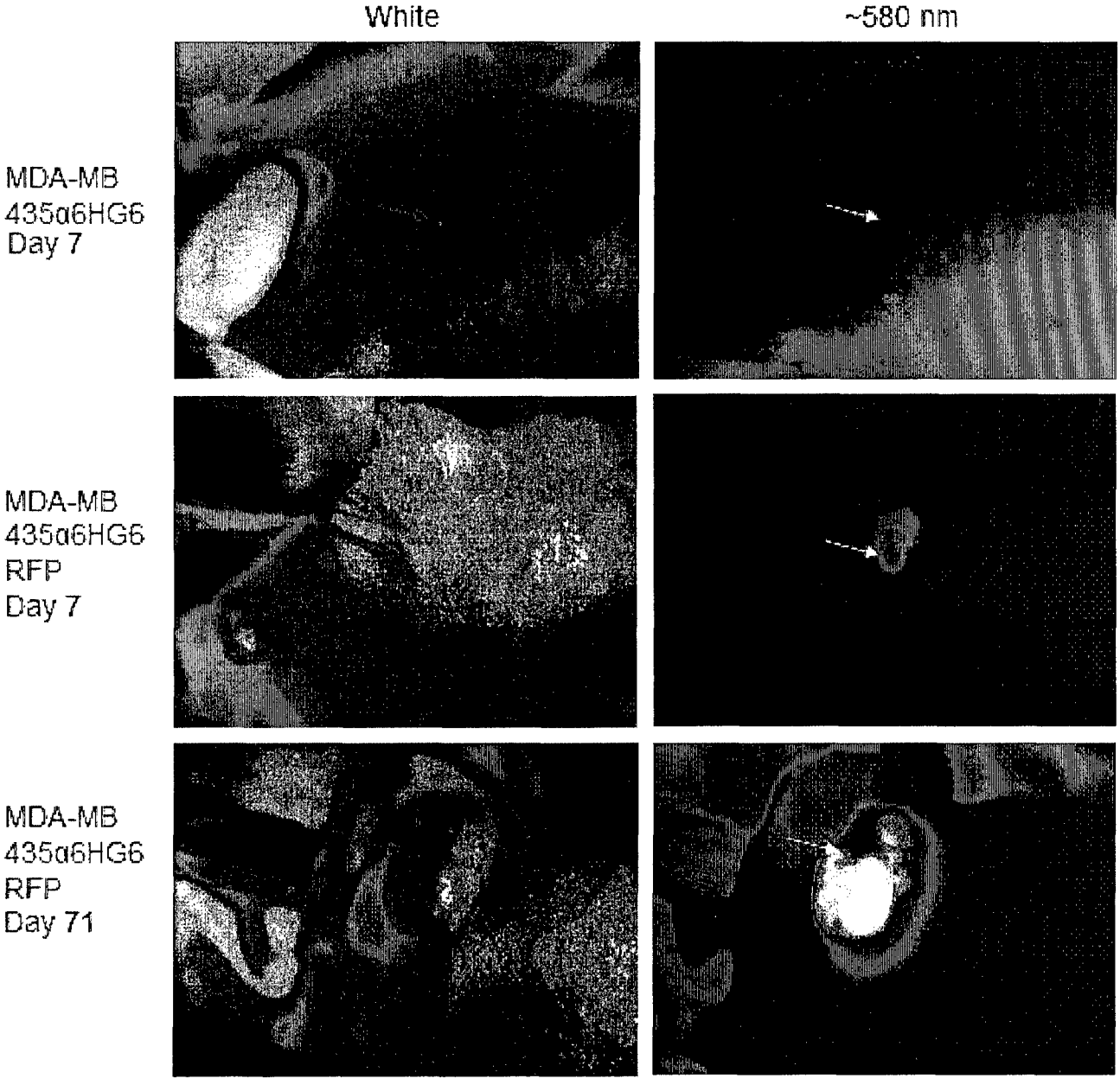

Fig. 6, Carlson, et al.

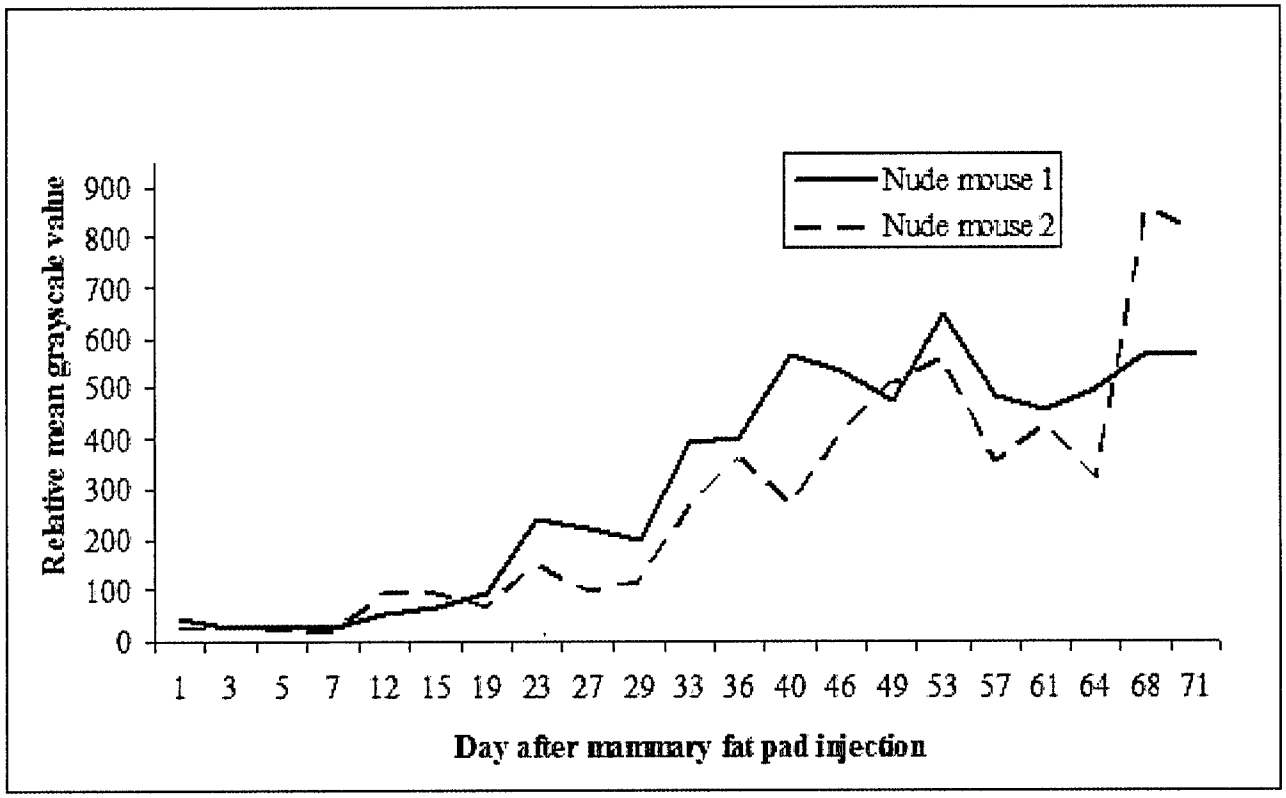

Fig. 7, Carlson, et al.

White

~ 580nm